Adaptive Hemodynamic Signal Estimation Using Kalman Estimator

Author

Basiq Warrad Quddusi

Registration Number

00000276654

Supervisor: Dr. Muhammad Jawad Khan

Department of Biomedical Engineering and Sciences

School of Mechanical & Manufacturing Engineering

National University of Sciences and Technology

H-12, Islamabad, Pakistan

May 2022

Adaptive Hemodynamic Signal Estimation Using Kalman Estimator

Author

Basiq Warrad Quddusi

Registration Number

00000276654

A thesis submitted in partial fulfillment of the requirements for the degree of

Master of Science in

Biomedical Engineering

Supervisor: Dr. Muhammad Jawad Khan

Thesis Supervisor's Signature: _____

Department of Biomedical Engineering and Sciences

School of Mechanical & Manufacturing Engineering

National University of Sciences and Technology

H-12, Islamabad, Pakistan

May 2022

FORM TH-4

National University of Sciences and Technology

MASTER THESIS WORK

We hereby recommend that the dissertation prepared under our supervision by **Basiq Warrad Quddusi** registration no. **00000276654** titled **"Adaptive Hemodynamic Signal Estimation Using Kalman Estimator"** be accepted in partial fulfillment of the requirements for the award of MS Biomedical Engineering degree with Grade (___)

Examination Committee Members

1. Name: Dr. Omer Gillani Signature: _____

2. Name: Dr. Asim Waris Signature: _____

3. Name: Dr. Hassan Sajid Signature: _____

Supervisor: Dr. Muhammad Jawad Khan Signature: _____

Co-Supervisor: Dr. Umar Ansari Signature: _____

_____ _____

Head of Department Date

COUNTERSIGNED

Date: _____ _____

Dean/ Principal

Thesis Acceptance Certificate

It is certified that final copy of MS thesis written by BASIQ WARRAD QUDDUSI registration no. 00000276654 of SMME has been vetted by undersigned, found complete in all aspects as per NUST Statutes/Regulations, is free of plagiarism, errors and mistakes and is accepted as partial fulfillment for the award of MS degree. It is further certified that necessary amendments as pointed out by GEC members of the scholar have also been incorporated in the said dissertation.

Signature with stamp: _____

Name of the supervisor: Dr. Muhammad Jawad Khan

Date: _____

Signature of HOD with stamp: _____

Date: _____

Countersigned by

Dean/Principal

Signature: _____

Date: _____

Declaration

I certify that this research work titled *"Adaptive Hemodynamic Signal Estimation Using Kalman Estimator"* is my own work. The work has not been presented elsewhere for assessment. The material that is used from other sources in this work has been properly acknowledged and referenced.

_____

Signature of Student

Basiq Warrad Quddusi

00000276654

Plagiarism Certificate (Turnitin Report)

This thesis has been checked for plagiarism. Turnitin report endorsed by supervisor is attached at the end of this report.

_____

Signature of Student

Basiq Warrad Quddusi

Registration Number

00000276654

_____

Signature of Supervisor

Dr. Muhammad Jawad Khan

Copyright Statement

Acknowledgments

In the name of Allah, the Most Gracious and the Most Merciful, all praises to Allah for the strengths and His blessings in completing this research work.

First, I would like to express my deepest gratitude to my supervisor Dr. Muhammad Jawad Khan whose guidance and support helped me a lot in completing my research work. His critical judgement in the form of comments and suggestions throughout my research work is one of the reasons behind the successful completion of this study.

I would like to extend my thanks to NUST and SMME for providing me with a decent research environment. I am thankful to my co-supervisor Dr. Umar Ansari and Guidance and Examination Committee (GEC) members, Dr. Omer Gillani, Dr. Asim Waris, and Dr. Hassan Sajid for providing me constant assistance throughout my research phase.

I would like to thank Principal of SMME and Head of Department of Biomedical Engineering, all the teachers and staff for their co-operations. Sincere thanks to all my class fellows especially Ali Raza Asif and Hassan Nawazish for the friendship.

I am extremely grateful to my parents (Mr. Muhammad Moin Quddusi and Mrs. Kausar Moin Quddusi) for their love, prayers, care, and sacrifices for educating and preparing me for my future. I am very much thankful to my siblings Dr. Hajrah, Mrs. Maarij, Mr. Nasik and Ms. Darrak; brother-in-law Dr. James and Mr. A. Muqsit for their love, understanding, prayers and continuous support to complete this research.

Dedicated to my parents and siblings for their tremendous support and cooperation.

Abstract

Functional Near Infrared Spectroscopy (fNIRS) is a technology that measures changes in the oxygenation level of blood present in brain whenever an activity is performed by human being. It is a non-invasive technique and uses near infrared light to detect changes in the concentration of two chromophores i.e., oxygenated and deoxygenated haemoglobin. During the recording, information related to neural activity in fNIRS signals gets compromised. This is due to the interference of noises from the environment outside as well as inside the human body. External noises can be light in the room and powerline noise. Internal noises are physiological noises such as cardiac, respiratory and mayer waves. Therefore, during analysis, it is required to remove these noises first and then extract main activity signal i.e., hemodynamic signal. Many techniques and methods have been proposed and practiced up to this date. Among them the most popular technique is General Linear Modelling (GLM). GLM models the signal by breaking it down into sum of all components present in the signal along with an error term. Previous studies and research that have used GLM for the reconstruction of activity signal used single frequency value for each noise but in reality, the frequency for each noise varies with the level of activity performed by the subject. This can lead to less accurate reconstruction of activity signal. In this study, this problem is kept under consideration and a method is developed to keep account for all the values of frequency that can corrupt fNIRS signal. Ranges of frequencies are considered instead of single values. These frequency ranges are first extracted using Continuous Wavelet Transform (CWT) and their possible magnitudes are estimated using Kalman filter. Similarly, activity signal is extracted from fNIRS signal using Discrete Wavelet Transform (DWT) and then its magnitude is estimated using Kalman filter. Output of these two steps is fed to GLM for reconstruction of possible hemodynamic signal. Results from this method are compared with the results of conventional GLM and significant improvement is observed both visually and statistically.

Keywords: Functional Near Infrared Spectroscopy (fNIRS), Hemodynamic Response Function (HRF), Continuous Wavelet Transform (CWT), Discrete Wavelet Transform (DWT), Kalman Filter (KF), General Linear Model (GLM).

Table of Contents

List of figures

List of Equations

List of Tables

Chapter 1: Introduction

Brain responds to the application of external stimuli or any change in the environment by encompassing various neurochemical reactions. This promotes local neuronal activity complemented with increased consumption of oxygen and glucose. This leads to a generous inrush of blood locally which is abundant in oxygen bound hemoglobin [1]. Mechanism of increased cerebral blood flow (CBF) locally is called neurovascular coupling [2]. Within several seconds amount of oxygenated hemoglobin (HbO) transported to the region of neuronal activity for utilization exceeds and becomes overabundant comparing to its counterpart deoxygenated hemoglobin (HbR) [3]. However, in the beginning of neural activity the amount of HbR becomes abundant in capillary bed as oxygen is drawn from HbO to meet the metabolization demands of glucose. This later feature of hemodynamic response is more difficult to measure than the first one [4]. The firm connection of the two properties (extent and locale) of neural activity with two properties (magnitude and locale) of the chromophores (HbO and HbR) serves as a quantifiable marker for neural activity [5]. Both HbO and HbR possess characteristic optical properties in near-infrared light thus, optical methods are used to measure changes in their concentration during neurovascular coupling [6].

1.1 Background

In 1977 Jöbsis first demonstrated and described the optical phenomenon of obtaining measurements of blood flow to the human cortex non-invasively [7]. This laid the foundation of functional Near Infrared Spectroscopy (fNIRS). Since then, it has been emerging in the field of optical imaging and attracting scientists from the fields of Brain Computer Interface (BCI), medical imaging and psychology[8]. It is a non-invasive technique that uses near infrared light to measure variations in the concentration of oxy-hemoglobin (HbO) and deoxy-hemoglobin (HbR) to give an effective reflection of activity taking place inside brain in response to a task performed by a person [1, 4, 9-13]. This optical brain imaging technique detects changes in HbO and HbR using visible (red)

and near-infrared light emitted and collected through sensors (source and detector) attached to the surface of the head [9].

Most biological tissues are transparent to light in the wavelength range of 700 to 1000 nm [14]. The wavelength for near infrared light used in commercially available fNIRS devices ranges from 685 to 850 nm , beyond this water absorbs majority of the photons hindering the optical results [15]. In fNIRS source optode incidents photons on the scalp, these photons pass through the skull and enter the top cortical regions. During their journey through head photons are scattered, reflected and some are absorbed by HbO and HbR. Unabsorbed photons are reflected back to the scalp following an elliptical (banana shaped) path and are collected by the detector optode. At the site of neuronal activity, the intensity of reflected light decreases with increase in concentration of HbO [16]. This happens due to higher absorption of photons by the increasing concentration of HbO in the locale of activity. The changes in the concentration of HbO and HbR at the site of neuronal activity are quantified using modified Beer-Lambert Law (MBLL) [1, 17-20].

$$OD(t,\lambda) = -log_{10}\left(\frac{I(t,\lambda)}{I_o(t,\lambda)}\right) = \sum_i \varepsilon_i(\lambda) c_i(t) DPF(\lambda) d + G(\lambda) \qquad \text{.....(1)}$$

Equation 1: Modified Beer-Lambert Law

Where, optical density (OD) is the function of time (t) and wavelength of light (λ) being used. It is the negative log of the ratio of attenuated light intensity (I) to initial light intensity (I_o). This negative relation is equal to summation of the product of molar extinction coefficient (ε_i), concentration of hemoglobin (c_i), differential pathlength factor (DPF) and distance between source and detector (d). (i) denotes total number of chromophores being investigated. Intensity of light lost due to scattering is represented with (G). In addition to optical density (OD) this equation can also be used to determine the scattering of light photons. Moreover, taking inverse log of light that has entered from source into scalp by the light gather detector optode yields concentration changes [10, 21].

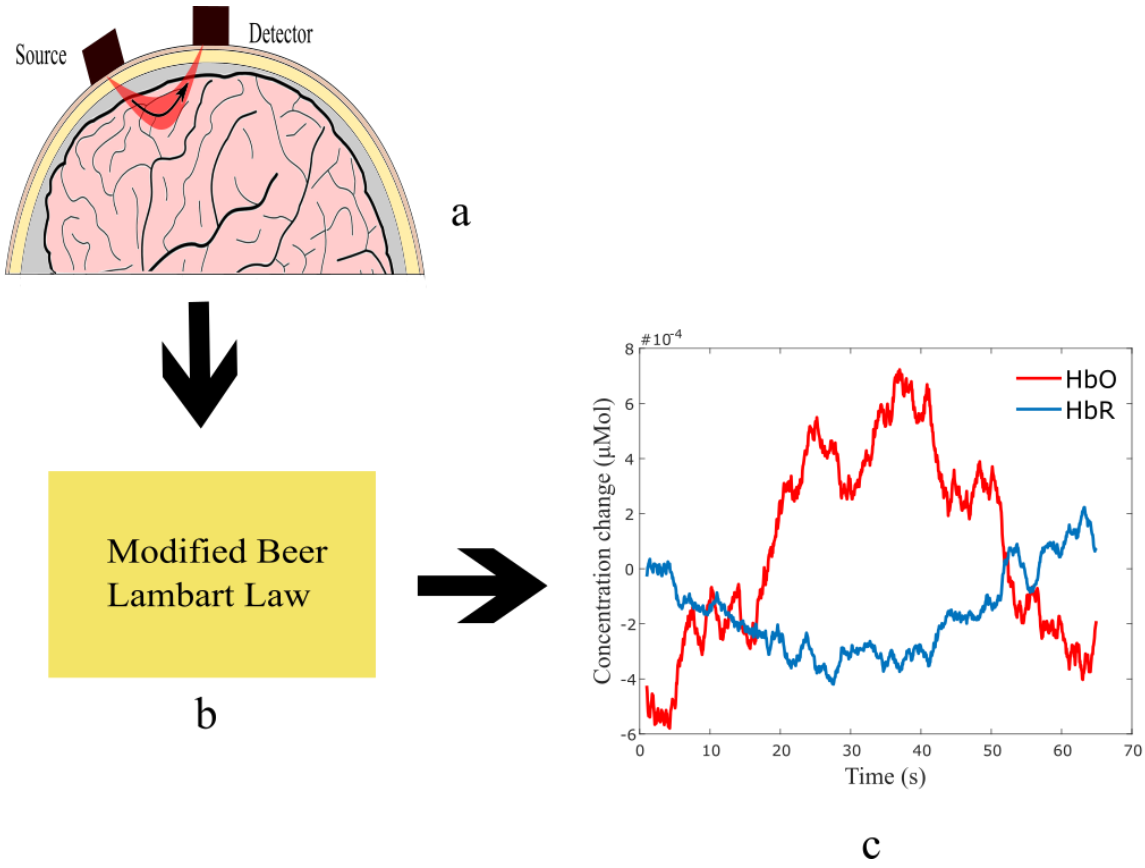

Figure 1: Graphical illustration for stages of fNIRS data acquisition

fNIRS signal obtained after the application of MBLL needs processing before it is used. This signal is raw in nature. The main activity signal is actually contaminated by the presence of motion artifacts, instrumental noise and physiological noises including cardiac signal, respiratory signal, and low frequency mayer waves. Presence of these noises makes hemodynamic signal impossible to be used. Therefore, removal of these noises become indispensable before taking any decision regarding brain functional activity on the basis of measured signals [22-25].

Different techniques had been used up to this date for reconstructing and removing activity based signal and noise respectively from this amalgam. Out of all these, General Linear Modeling (GLM) has a decent reputation and has been used repeatedly [26]. GLM is a technique that has been used widely in the field of brain imaging to reconstruct the Hemodynamic Response Function (HRF) from fNIRS and functional Magnetic Resonance Imaging (fMRI) signals [27]. GLM models brain activity by taking sum of all

the components of measured signal i.e., noise and functional part of signal [8, 28]. Accurate estimation of activity signal relies heavily on the correct estimation of their magnitudes and features such as baseline correction and removal of motion artifacts and physiological noise.

In this study, wavelet transform and Kalman filter based GLM has been used to model fNIRS signal. Continuous Wavelet Transform (CWT) has been used to separate physiological noises from the measured signal. Hemodynamic Response Function (HRF) depicting brain activity has been modeled using three gamma functions. Discrete Wavelet Transform (DWT) has been used to extract most part of the activity signal from the measured signal. Kalman filter has been used to estimate the magnitudes of all the components that has to be used in GLM.

1.2 Problem statement

The current brain images are made using the General Linear Model. The hemodynamic signals and their noises are treated as linear entities. However, the behavior of hemodynamics varies with the changing noise. This causes problem in accurate estimation of hemodynamic responses that contributes to the formation of brain images. An adaptive method is required that can model varying noises and hemodynamic signal.

1.3 Objectives

Given below are the objectives of this study.

- Extraction of noise from fNIRS signal using continuous wavelet transform.
- Estimation of varying noise components of fNIRS signal using Kalman estimator.
- Incorporation of non-linear noise components in General Linear Model (GLM) to minimize the noise completely out of desired HRF.
- Generation of brain activation maps.

1.4 Areas of application

Current study targets the following areas of application.

- Brain Computer Interface (BCI)
- Biomedical Industry
- Diagnosis of brain diseases

1.5 Thesis overview

In this thesis, Chapter 1 is pure introduction about fNIRS signal and its estimation. Chapter 2 covers the literature review regarding the problem statement, and its provided solutions in the past. Chapter 3 provides with the methodology proposed in this study and how it is performed step by step. Chapter 4 is about results from the proposed methodology. Chapter 5 is about conclusions that has been drawn from the whole study and also imparts future work.

Chapter 2: Literature Review

Raw or unprocessed fNIRS data has several elements of noise such as physiological noise (i.e., cardiac waves, respiratory waves and mayer waves), instrumental noise and motion artifacts. These noises attenuate the functional part of the cortical signal thus, making it hard to discover. Pre-processing aids in the removal of the above mentioned noises. After pre-preprocessing, Hemodynamic Response Function (HRF) is acquired from raw data using processing techniques. Therefore, this raw data needs to be pre-processed and processed before any conclusion is drawn from it regarding task related cortical signal [26].

fNIRS is gaining popularity in the field of research due to its noticeable low cost and easy portability as compared to fMRI. Superficial nature of motor cortex and portability of fNIRS device have motivated majority of the researchers to keep the focus of their studies on motor activities [29-34].

HRF used in fNIRS studies is quite comparable to blood oxygen level dependent (BOLD) model used in functional Magnetic Resonance Imaging (fMRI) [26, 29, 35, 36]. Due to this HRF is modeled using two and three gamma functions [37] whose basics are borrowed from studies of fMRI.

Rise in the popularity of fNIRS has caused the proposition of many pre-processing and processing techniques. Selection of suitable technique for one's study has become quite challenging [26].

Conventional filtering is a popular technique to eliminate physiological noise from fNIRS data. Selection of filter and their coefficients vary from case to case. Correct selection of filter type is important as it can cause loss of activity signal [23-25]. Finite Impulse Response (FIR) and Infinite Impulse Response (IIR) filter are two filters that are generally used to remove physiological noise [26, 38].

In [39-42] physiological noises are removed using low pass filter with a specific cut off frequency. Motion artifacts are removed using wavelet motion correction. Remaining linear and non-linear noises are removed by fitting a polynomial of order 3 to fNIRS

signal and then it is subtracted from main data. In [39] HRF is derived by averaging the signal in time domain.

In [43, 44] Butterworth band pass filter was used to remove the high and low frequency noise. Cut off frequency for each trial was set different because the length of all trials was not same. Moreover, in [43] a three gamma function has been used to model canonical HRF (cHRF).

In [45-47] physiological artifacts are removed using a fourth order zero phased low-pass Butterworth filter. The cutoff frequency used was 0.3 Hz to eliminate high frequency artifacts. HRF in [45] has been calculated by taking average spatially.

In [48] signals underwent the filtration between two frequencies 0.01 and 0.7 Hz. First filter was an IIR 9th order Butterworth filter with 0.1 Hz of cutoff frequency. This was then convolved with an FIR low- pass filter with cutoff frequency of 0.7 Hz.

According to [49, 50] some of the physiological noises resides in the frequency range where activity signal may exist. In such a case applying band pass, high pass and low pass filter may become the reason behind the loss of some part of activity signal leading to inaccurate estimation of HRF.

Other than filtering there exist many methods to remove physiological noise and motion artifacts from raw fNIRS data. In [51, 52] wavelet coherence was applied to fNIRS signals. Physiological noises behaving similarly in all signals are located and masks are generated using image processing techniques. Then mask was run over the scalogram of wavelet transform of each signal. This suppressed the area under the mask which was supposed to be noise and then remaining coefficients were converted back into signals.

Another effective method for removing physiological noise from raw fNIRS signals is short source-detector distance channel (sSD channel) based correction [51, 53-58]. In this technique a short source-detector is placed between the long source and detector. This short S-D has a distance of almost 0.5 cm to 1.5 cm [59-61]. Due to short distance between the source and detector, the near infrared light entering the head is now constrained to the superficial layers instead of reaching the cortex. As this signal does not reach the cortex thus, it carries no representation of the activity signal, instead it is assumed that this signal contains the representation of all the physiological noises in it. Therefore, information received from short S-D signal is used to remove the noise from

normal source detector channels. Although it is an effective method, yet it has its shortcomings. Short S-D is not supported by all fNIRS devices. Moreover, setting this up takes some decent amount of time. Ideally it may look like the complete solution, but physiological noise is not homogeneously distributed over the scalp which means the more short S-D in numbers the better, but channels for fNIRS are usually limited in numbers. Therefore, this method still needs optimization [56, 60].

Another method for removing physiological noise from fNIRS signals is blind source separation (BSS) techniques or algorithms. The two main methods that have been used widely in fNIRS are principal component analysis (PCA) [62-64] and independent component analysis (ICA) [65, 66]. In these two methods fNIRS signal is decomposed into its components based on the source from where they can be originating. This is performed using assumptions which can be either orthogonal assumption in case of (PCA) or statistical independent assumption in (ICA). After this, components are expressed in the form of energy densities and their spatial uniformity is checked and on the basis of several assumptions about noises they are separated from the signal [67].

In [64] author used Principle Component Analysis (PCA) to remove physiological interference and motion artifacts and block averaging is used to derive HRF. In [68-70] independent component analysis (ICA) has been used for the removal of physiological interference and motion artifacts.

In [71] recursive least square estimation (RLSE) has been used for removing physiological noise as well as motion artifacts. Usually, fNIRS signal is mathematically modeled as a linear summation of different constituents which mostly are activity part of fNIRS signal, physiological noises residing in raw signal and a component that helps in the modeling of baseline drift in fNIRS signal. RLSE is a method that recursively contributes by making an estimate of the amplitudes for the above mentioned components on the basis of cost function and a forgetting factor.

GLM is used to model and remove the activity signal and noise respectively. In GLM, signal is modeled as a sum of activity part, physiological noise and an error term. Its regressors are estimated by different estimation techniques such as Kalman filter (KF) [13, 72], RLSE [73], Extended Kalman Filter (EKF) [8] and Cholesky-decomposition based recursive least square [74].

Apart from physiological noise there are motion artifacts in the signals which are caused by movement of the head or optode placed on the scalp. This appears as sudden spikes or surges in fNIRS signals. Sometimes these artifacts make the signal move away from the base line and cause the phenomenon of baseline drift. There exist many methods to remove these artifacts from the signal but the most practiced one is that presented in [75]. This method uses wavelet transform to remove motion artifacts. According to that study two types of wavelet coefficients were acquired. Type one was those of activity signal, type two; those representing the motion artifacts. It was stated that type one coefficients had gaussian distribution with small covariance and if larger covariance was observed then those must be type two coefficients i.e., motion artifact coefficients. Type two coefficients were suppressed to zero after differentiating them from type one coefficients. Then inverse wavelet transform of the remaining coefficients was taken. In this way motion artifacts were removed from the fNIRS signal.

Other than the one discussed in above paragraph, [76] proposed to remove the entire segment from the signal that contains motion artifact. This method requires visual attention of the one performing experiment to identify the motion artifact in the recorded signal.

Many studies have suggested the use of adaptive filtering [53, 77, 78] for removing motion artifacts from the fNIRS signal. These studies have one thing in common and that is an auxiliary signal (that needs extra setup) to serve as a reference signal which has correlation with motion or physiological nuisance.

Chapter 3: Methodology

This chapter focuses on the methodology used to develop the approach. Data was collected using fNIRS device. All the pre-processing and processing have been done using MATLAB 2018b. Firstly, cHRF is modeled using gamma function, then using wavelet transform raw signal is broken down into its constituents. Using previous knowledge from literature review, activity signal and noises are separated. Following the separation, these signals are used as input for GLM. Regressors for aforementioned signals in GLM are estimated using Kalman Filter. After this brain activation maps are formed.

3.1 Experimental Setup

3.1.1 Data

The fNIRS data used in proposed study comprises of five healthy subjects. All of them were right handed male. The data was collected from motor cortex. Each signal has 3908 data points. The data was collected at a sampling frequency (F_s) of 15.625 Hz. Data was acquired from 16 channels.

3.1.2 Experimental Procedure

Before starting experiment, every subject was seated on a comfortable chair asked to relax himself. His hand was rested on a table. In the beginning, subject was asked to stay calm and do nothing for 20 seconds. This was initial rest. After that he was asked to tap his right hand index finger for 20 seconds and then take rest for 20 seconds. This whole procedure was repeated 5 times and after performing task for fifth time there was a rest of 50 seconds. Thus, total length of time was 250 seconds. Figure 2 shows the experimental paradigm.

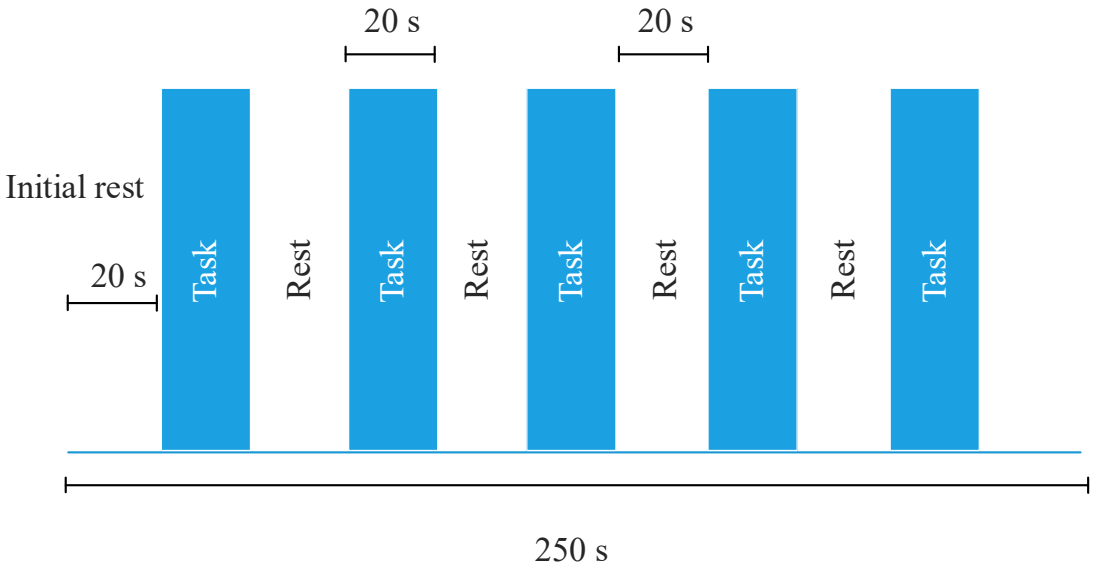

Figure 2 : Stimulating Paradigm

3.2 Channel Selection

Selecting the active channels and discarding the inactive channels is very important. In this study Channels are selected on the basis of t-values. In MATLAB *robustfit* command has been used to calculate t-values and channels with higher t-values are considered i.e., channel 3, 10, 11 and 12.

3.3 Canonical HRF (cHRF)

In proposed study HRF has been modeled using three gamma function mentioned in [37]. Three gamma function is considered because of its ability to incorporate initial dip. Figure 3 shows HRF made using three gamma function.

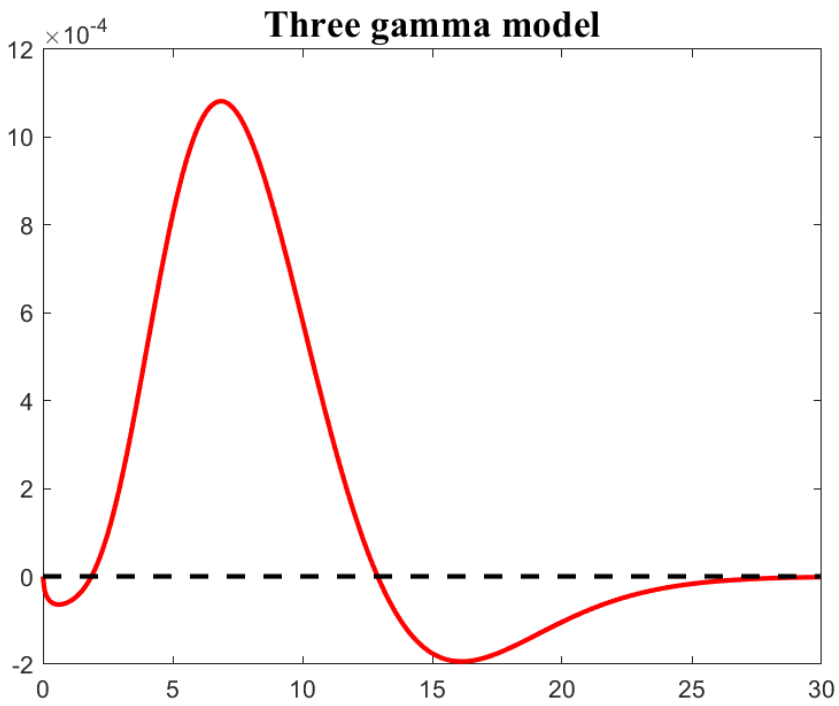

Figure 3 : cHRF using three gamma functions

After the modeling of HRF, it is convolved with a box car function of stimulus i.e., stimulating paradigm. This convolution results in the formation of cHRF or Oxy-HRF. This relation can be written simply in the form of following equation.

$$O = g * l \dots\dots\dots\dots (2)$$

Equation 2 : Convolution of cHRF and stimulating paradigm

Where O represents HbO, g represents three gamma function and l represents vector of stimulus. **Figure 4** shows convolution of HRF and stimulating paradigm.

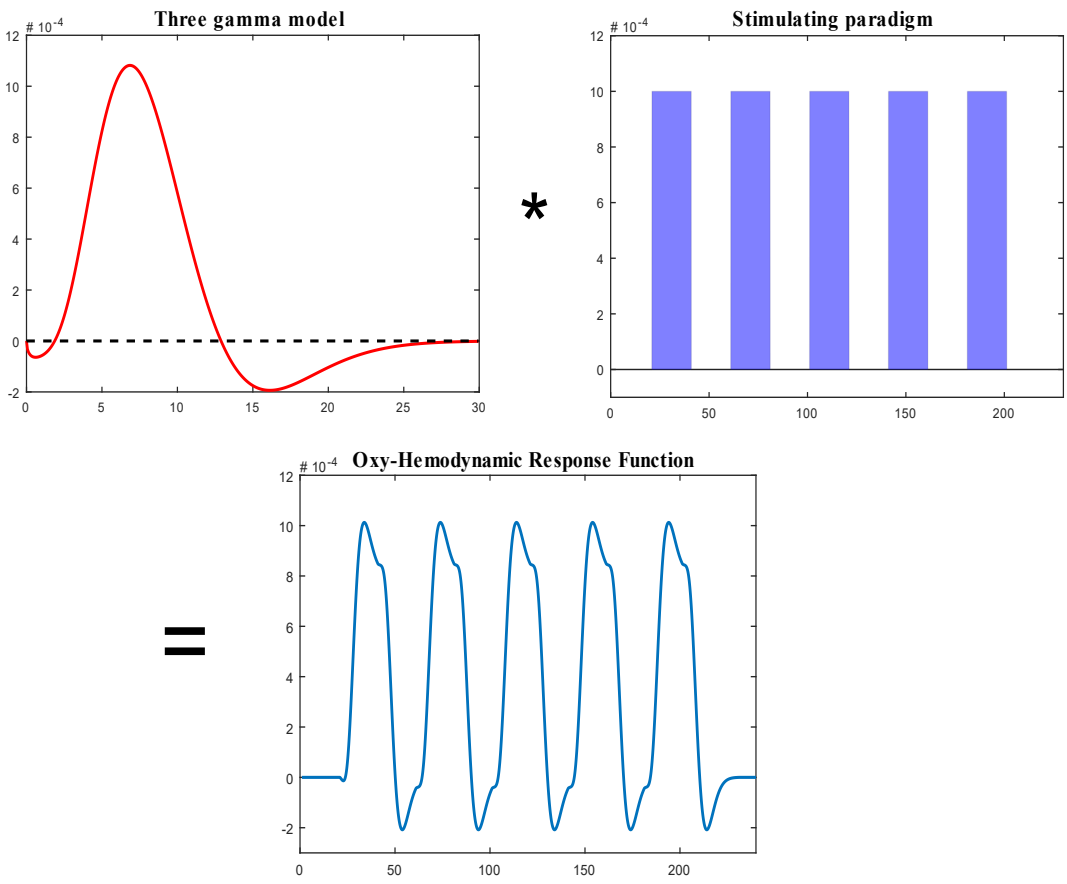

Figure 4 : Convolution between three gamma base HRF and stimulating paradigm

3.4 Frequency extraction

Continuous wavelet transform (CWT) is applied to the raw signal in MATLAB. Following that, A two dimensional matrix ***wt*** and a column matrix ***f*** is obtained. ***wt*** contains wavelet coefficients for the signal. Each row corresponds to one scale. Column matrix ***f*** contains the frequencies captured by each scale. Frequencies along with their wavelet coefficients are then divided in to seven groups on the basis of frequency ranges. Following are the groups of frequencies.

1. Cardiac frequencies ranging from 0.8 Hz to 1.2 Hz [79].
2. Respiratory frequencies ranging from 0.3 Hz to 0.6 Hz [79].
3. Mayer wave frequency i.e., 0.1 Hz [79].
4. Unknown frequencies group 1 (UG 1) below 0.1 Hz.
5. Unknown frequencies group 2 (UG 2) ranging from 0.11 Hz to 0.29 Hz.

6. Unknown frequencies group 3 (UG 3) ranging from and 0.61 Hz to 0.79 Hz.
7. Unknown frequencies group 4 (UG 4) above 1.2 Hz.

Signals for each group of frequencies were reconstructed by taking inverse wavelet transform of their wavelet coefficients. After that a single signal is made from each group by taking sum of all the signals from that group.

$$S_x = \sum_{k=1}^{n} s_k \quad \ldots\ldots\ldots (3)$$

Equation 3 : Shows summation of reconstructed signals

Where S_x represents summed up signal, *x* can be any of these cardiac, respiratory, mayer and other frequency group. s_k represents signal of particular frequency and *k* represents number of signals in the group.

3.5 Extraction of functional part

Discrete wavelet transform (DWT) is applied to raw data for extracting the functional part of the hemodynamic signal. In proposed study, discrete wavelet transform is applied to raw signals using *Wavelet Analyzer* application in MATLAB. Daubechies wavelet of order 7 is employed as mother wavelet [80]. DWT decomposes a signal into approximated component and detailed components. Lower detailed components capture high frequency information while higher detailed components capture low frequency information. A level three discrete wavelet transform is shown in **Figure : 5**. S(t) is signal which is decomposed into its approximation a1 and details d1. Then in second level a1 is decomposed into a2 and d2 and in third level a2 is decomposed into a3 and d3. This is an illustration of how levels and then output of discrete wavelet transform are formed. In this study, level ten discrete wavelet transform has been used.

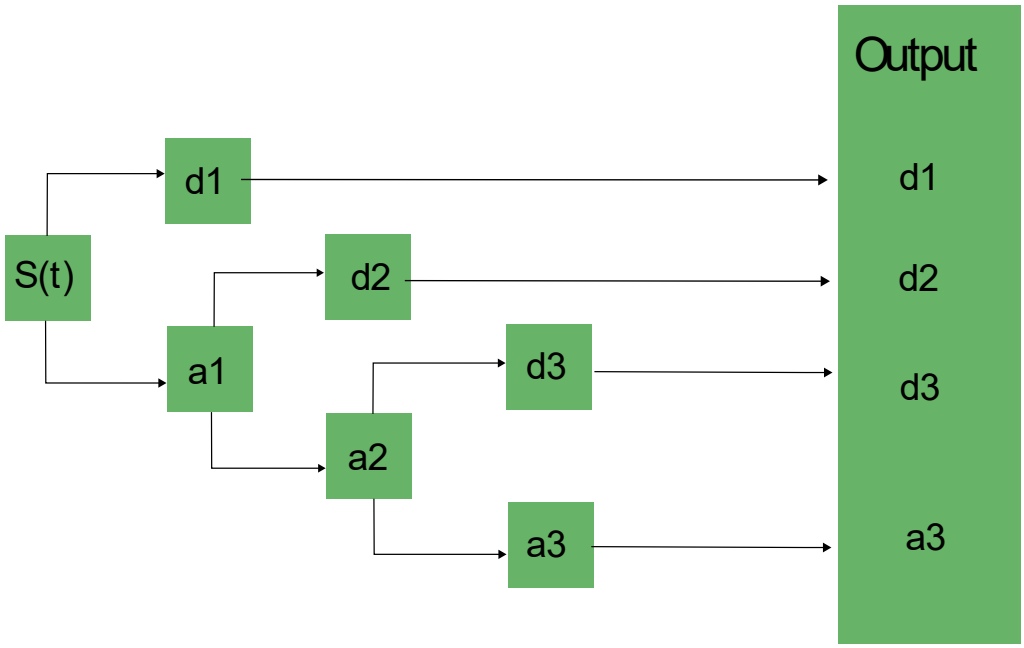

Figure 5: A level 3 discrete wavelet transform

In our study single task frequency was 0.05 Hz (1/time for single task). Thus, detailed components from level 7 to 10 are summed up to form single signal. This signal is our activity signal whose magnitude will be estimated.

3.6 Estimation using KF

Kalman Filter is a technique that practices recursive estimation and updates the estimates on the basis of previous state of system [81]. Due to its durable estimation, use of Kalman filter is practiced widely in different fields of study [82]. In present study, Kalman filter is used to estimate the physiological noise and magnitude of HRF. Instead of doing a parallel estimation for all channels, estimation has been done point by point for each channel in time series.

For any given channel equations for state vector, transition and observation can be given respectively

$$X(k) = [\beta_1\,(k)\,\beta_2\,\,(k)\,\ldots\beta_n(k)]^T$$

Equation 4: State vector

$$X(k) = AX'(k-1) + w(k)$$

Equation 5: State equation

$$y(k) = G(k)X(k) + v(k)$$

Equation 6: Observation equation

Here A is transition matrix, G is matrix for explanatory variables, w is process noise and v is observation noise.

3.7 General Linear Modeling (GLM)

In proposed study, hemodynamic signal is modeled using GLM. It takes and explains data in a linear combination of variables along with noise. The basic equation explaining GLM is as follows

$$y(t) = H\,\beta + \,\varepsilon$$

Equation 7 : GLM

Here *H* is the design matrix that contains all the variables to model hemodynamic response, β is a column matrix of regressors for GLM, ε represents error and *y(t)* denotes measured signal.

In proposed study, design matrix *H* is made of following constituents.

$$H = \begin{bmatrix} HRF & \Delta HRF & \Delta^2 HRF & sin2\pi f_{car}t & sin2\pi f_{res}t & sin2\pi f_{may}t & sin2\pi f_1 t & \cdots & sin2\pi f_n t \\ \vdots & \vdots & \vdots & \vdots & \vdots & \vdots & \vdots & \vdots & \vdots \\ \vdots & \vdots & \vdots & \vdots & \vdots & \vdots & \vdots & \vdots & \vdots \\ \vdots & \vdots & \vdots & \vdots & \vdots & \vdots & \vdots & \vdots & \vdots \end{bmatrix}$$

Where, sin2πft represents signal of specified frequency ranges. In this,

$f_{car} =$ cardiac frequency

$f_{res} =$ respiratory frequency

f_{may} = mayer frequency

$f_{1\ to\ n}$ = remaining random frequencies

HRF is the activity signal extracted using DWT and KF, Δ HRF and Δ^2 HRF are first and second order derivatives of HRF.

3.8 Algorithm

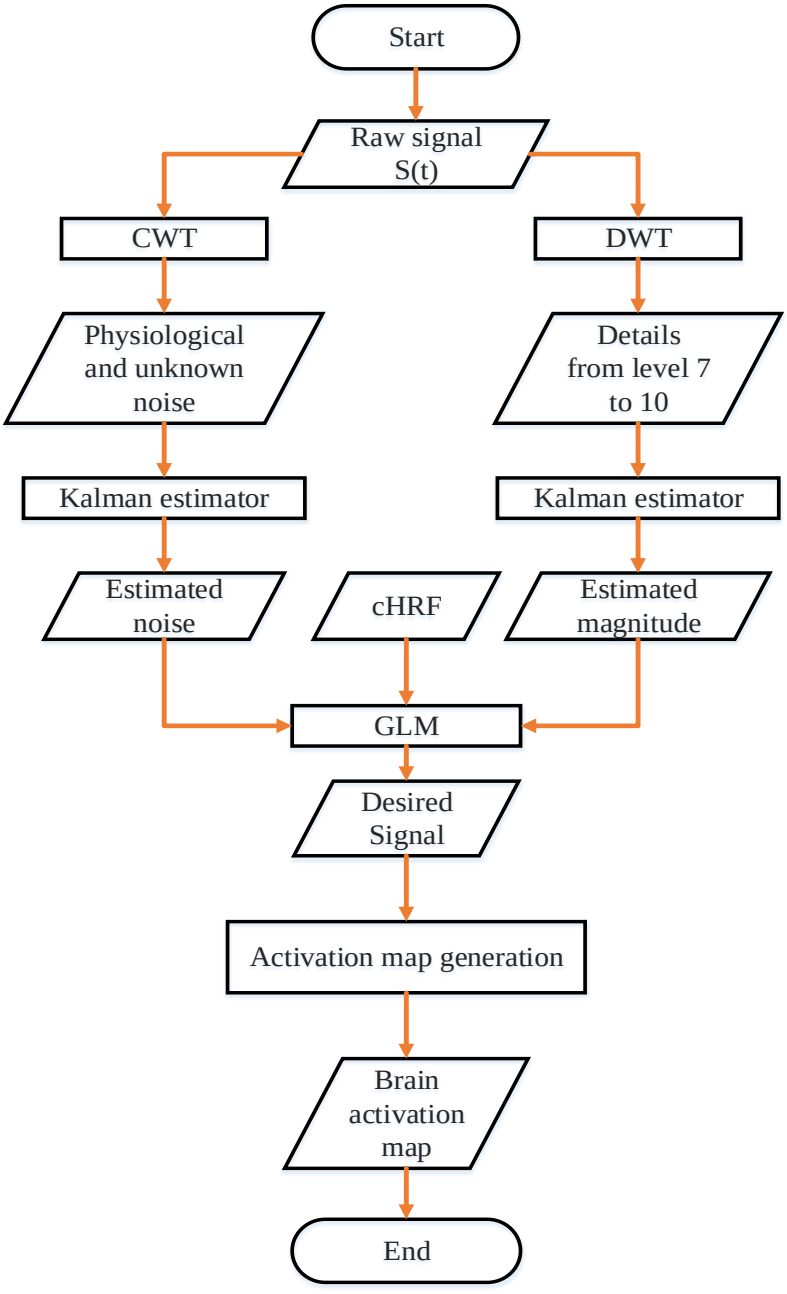

Figure 6 : Algorithm of proposed study

Chapter 4: Results and Discussion

This chapter of thesis provides with the results acquired by implementing the methodology proposed and explained in previous chapter.

4.1 Results from CWT

CWT yields column matrix of frequencies and a two dimensional matrix containing coefficients for these frequencies. In the figure given below it has been shown coefficents of wavelet transform captured by scale.

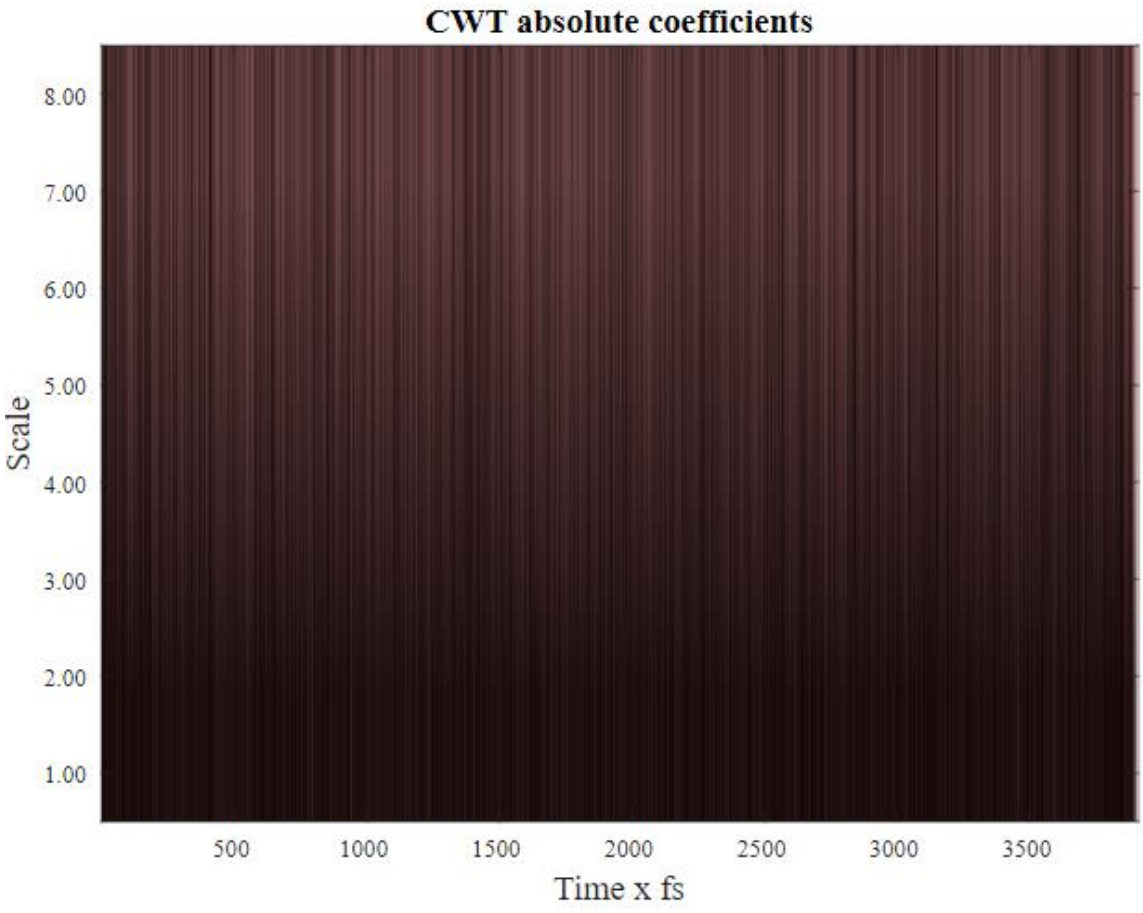

Figure 7: Absolute wavelet coefficients of raw signal

4.2 Results from DWT

Discrete wavelet transform has been applied to the signal for the identification of activity signal. The results in **Figure: 8** shows eleven graphs for eleven signals. Out of which from $\mathbf{d_1}$ to $\mathbf{d_{10}}$ are details for the raw fNIRS signal whereas, $\mathbf{a_{10}}$ is the level 10 approximation. It can be seen that as the level of details increases, the frequency captured by it decreases that is why $\mathbf{d_1}$ has highest frequency content and $\mathbf{d_{10}}$ has the lowest frequency content.

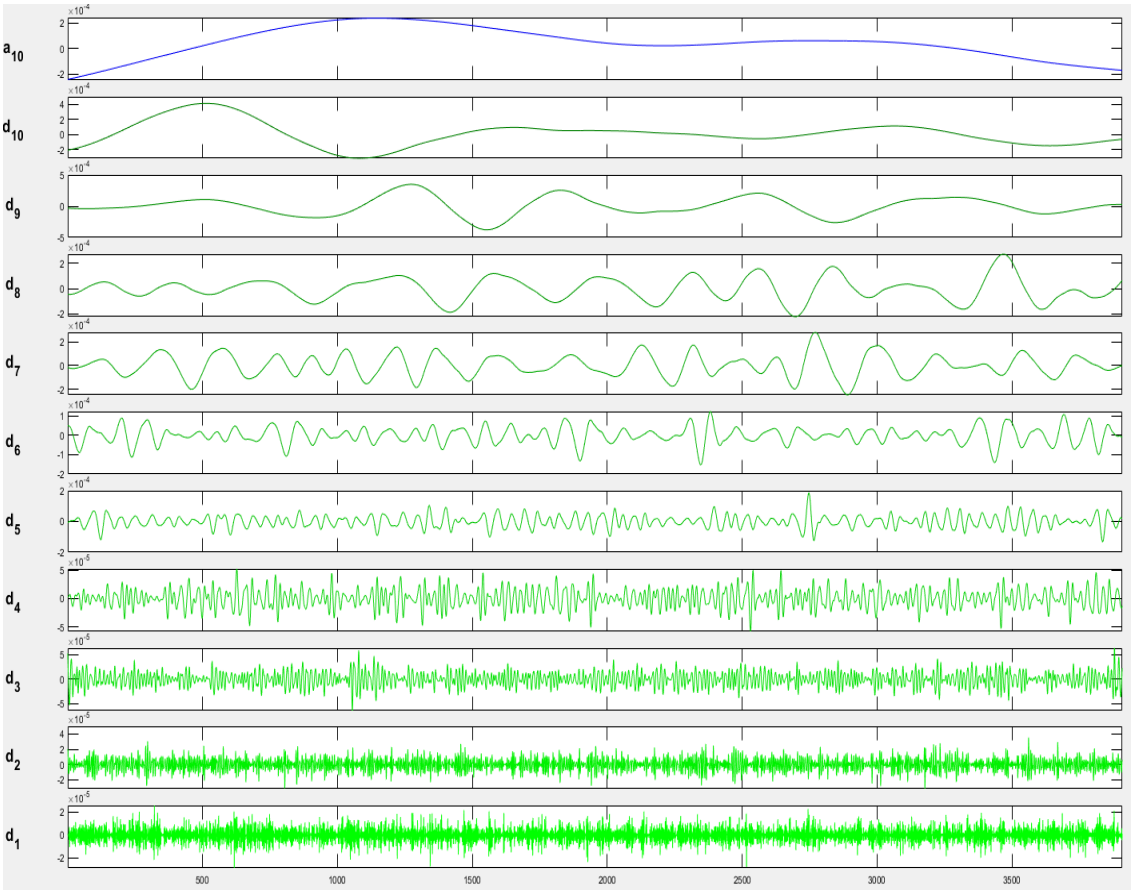

Figure 8: Result of DWT

4.3 Results from Kalman Filter

Signals from processes of frequency extraction and functional part extraction are now introduced to Kalman filter for the estimation of their magnitudes and regressors.

Following are the results showing the effect of KF on cardiac, respiratory, mayer and other unknown frequency group signals from channel 3 of subject 3 as well as functional part obtained from DWT.

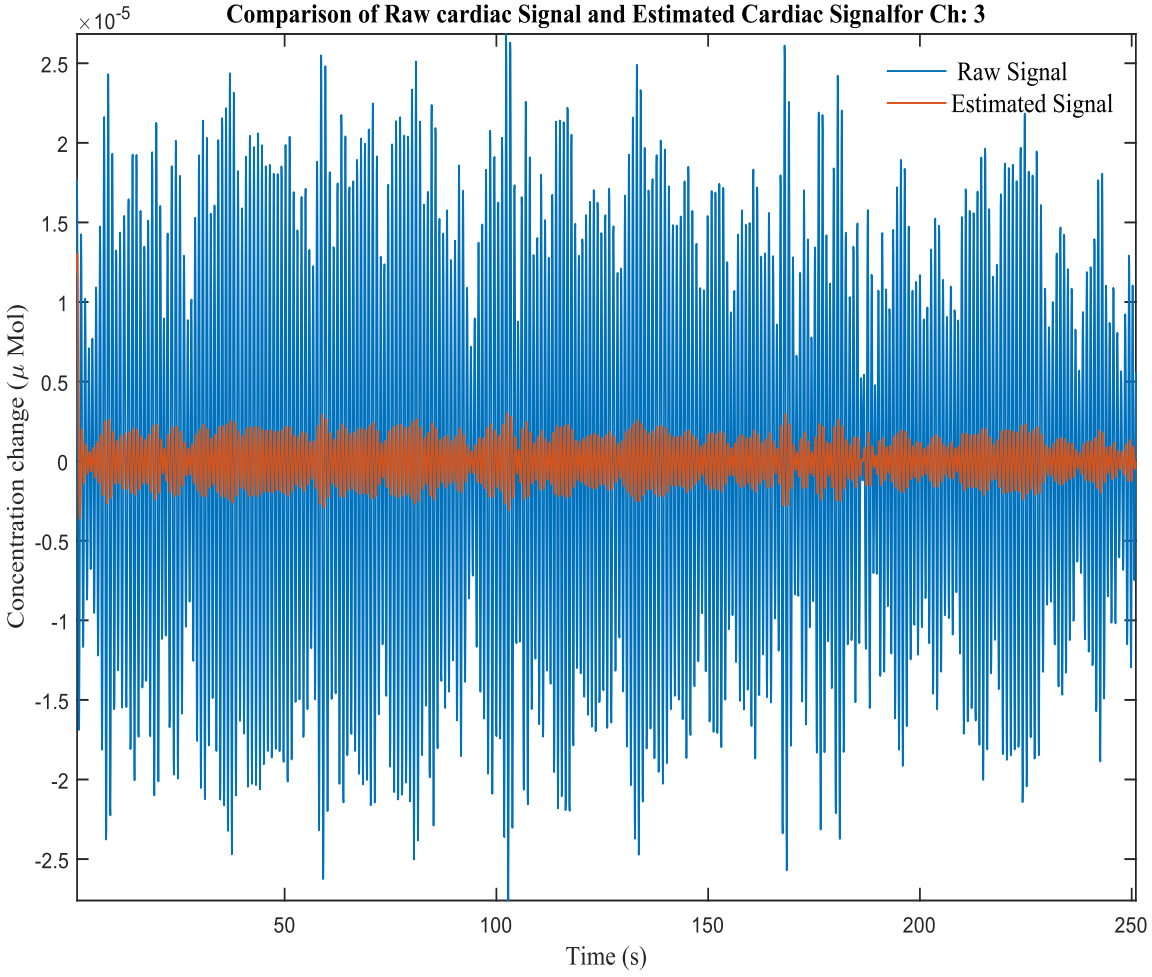

Figure 9: Cardiac signal before KF (blue) and after KF (orange)

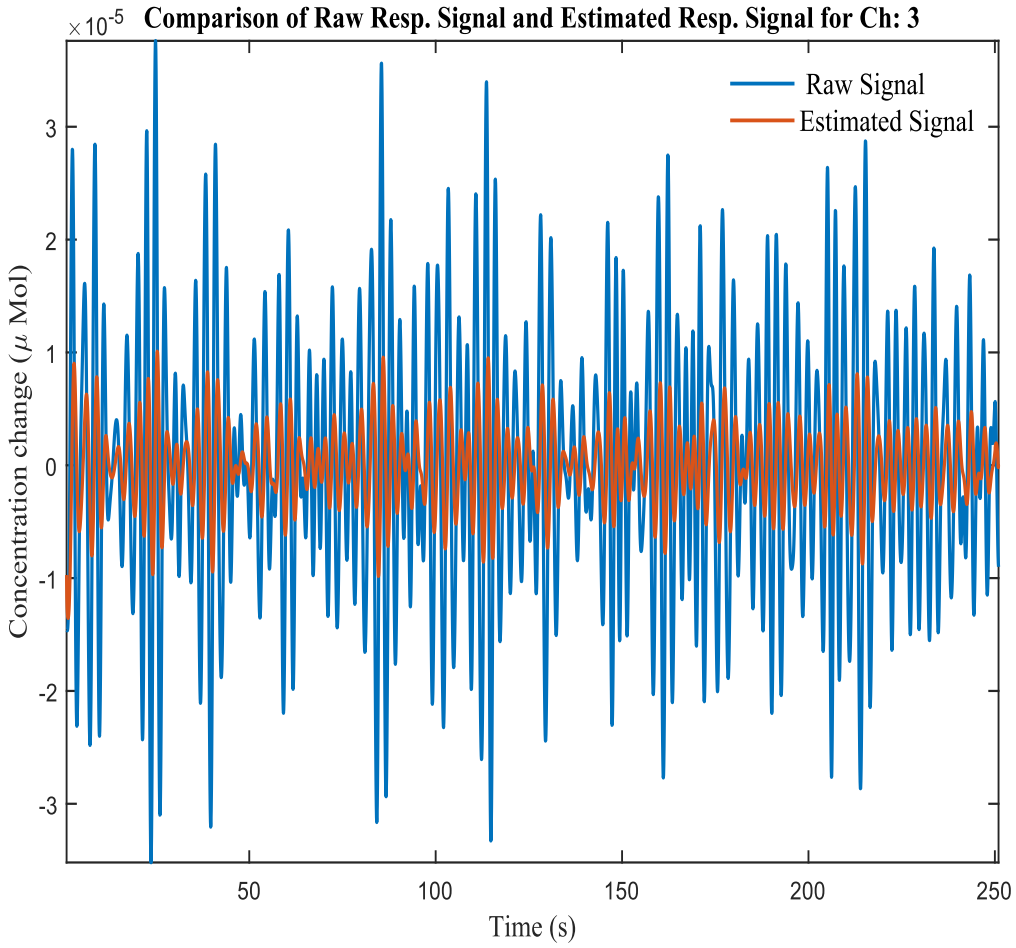

Figure 10: Resp. signal before KF (blue) after KF (orange)

In **Figure: 10** it can be observed that before undergoing the process of Kalman estimation Respiratory signal has different magnitude. Kalman filter estimates the magnitude keeping account of the presence of measurement and process noise that can create or cause uneven increase or decrease in the magnitude of the signal. Ratio of process noise to measurement noise used in the estimation is 1:10. Therefore, estimated magnitude is less than the original magnitude.

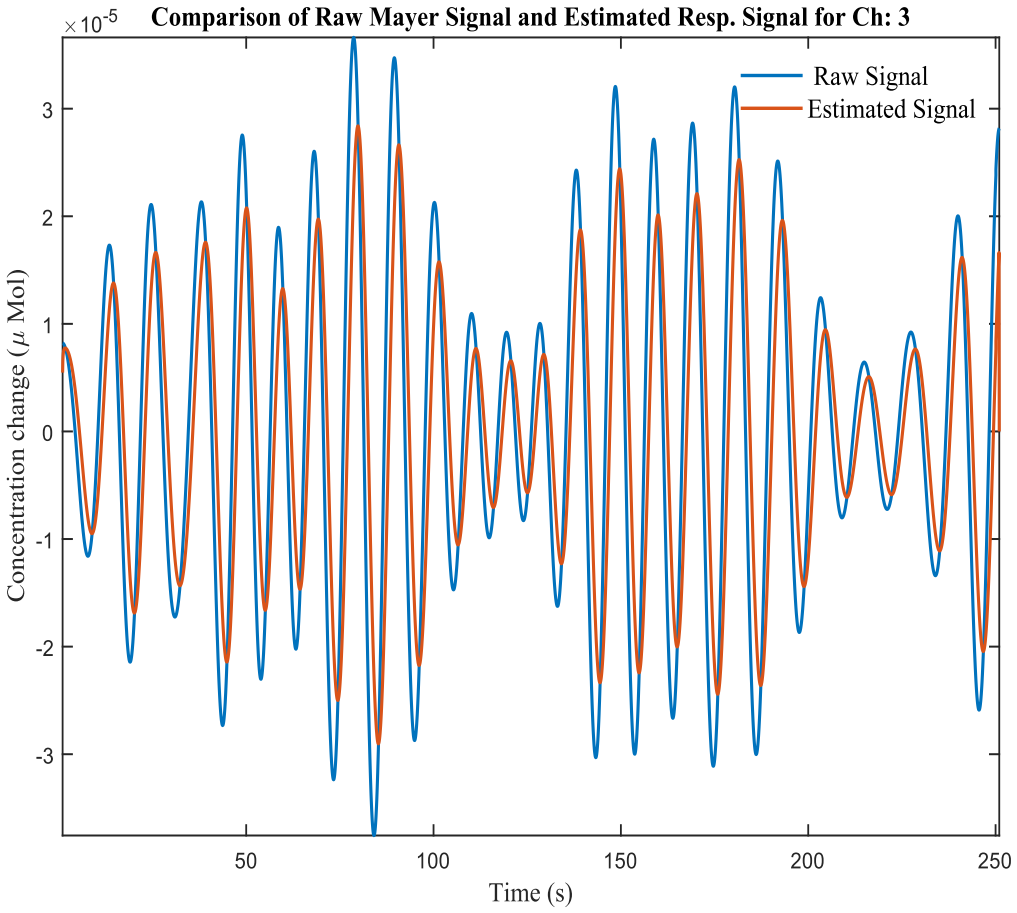

Figure 11: Mayer signal before KF (blue) and after KF (orange)

In **Figure: 11** it can be observed that before undergoing the process of Kalman estimation raw mayer signal has different magnitude. Kalman filter estimates the magnitude keeping account of the presence of measurement and process noise that can create or cause uneven increase or decrease in the magnitude of the signal. Ratio of process noise to measurement noise used in the estimation is 1:10. Therefore, estimated is slightly less than existing magnitude.

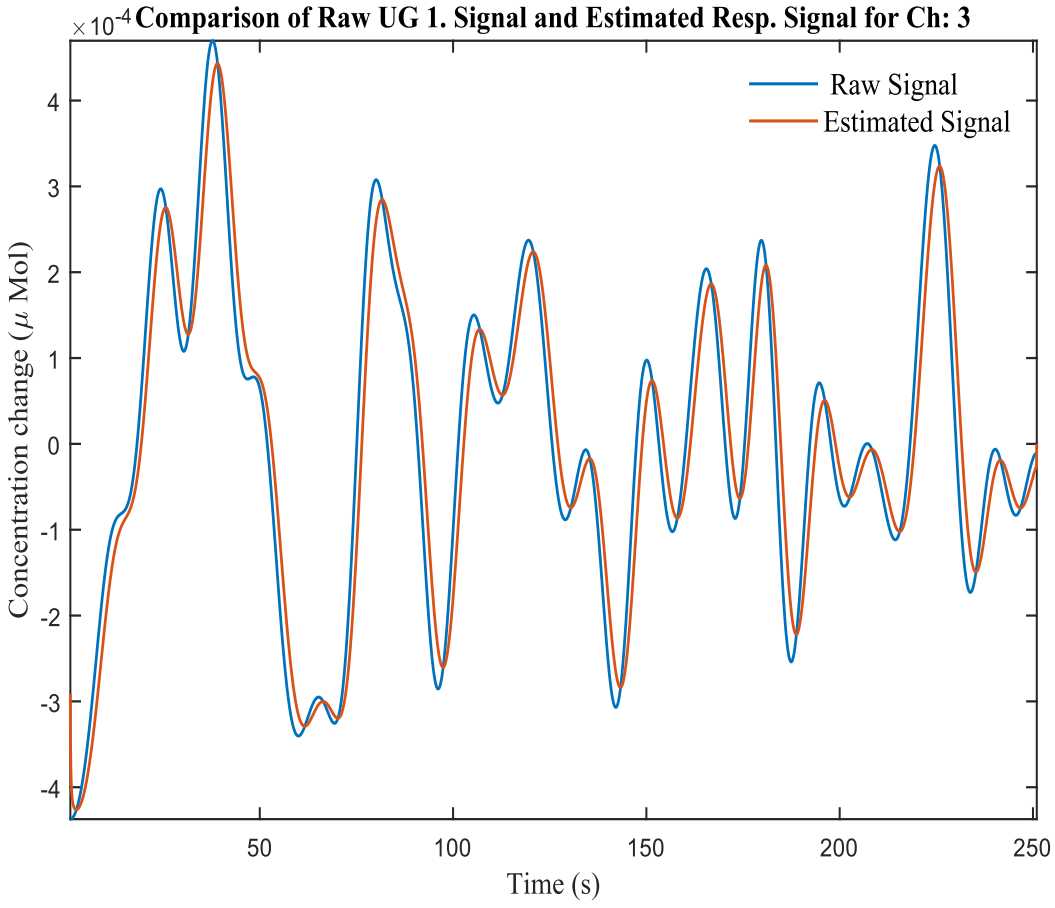

Figure 12: UG.1 signal before KF (blue) and after KF (orange)

In **Figure: 12** it can be observed that before undergoing the process of Kalman estimation UG 1 signal has different magnitude. Kalman filter estimates the magnitude keeping account of the presence of measurement and process noise that can create or cause uneven increase or decrease in the magnitude of the signal. Ratio of process noise to measurement noise used in the estimation is 1:10. Therefore, magnitude estimated is close to the existing one.

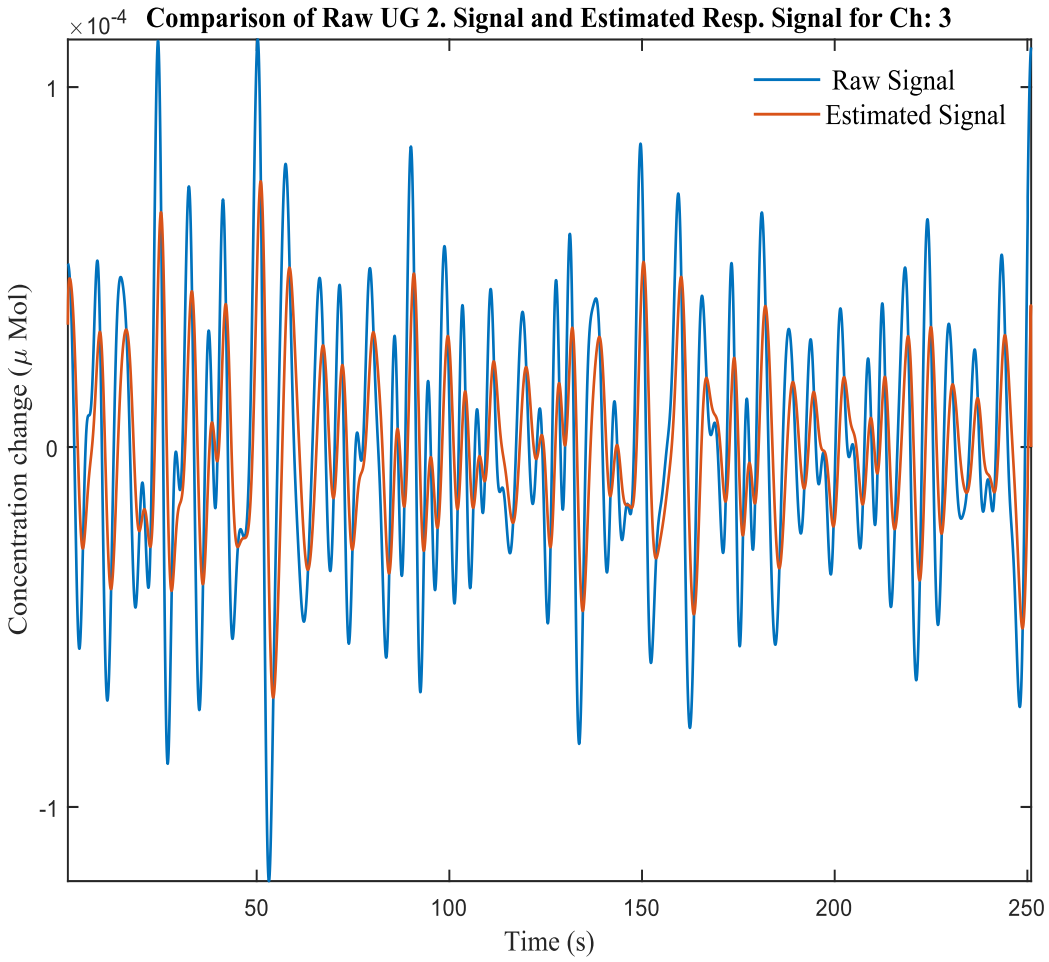

Figure 13: UG.2 signal before KF (blue) after KF (orange)

In **Figure: 13** it can be observed that before undergoing the process of Kalman estimation UG 2 signal has different magnitude. Kalman filter estimates the magnitude keeping account of the presence of measurement and process noise that can create or cause uneven increase or decrease in the magnitude of the signal. Ratio of process noise to measurement noise used in the estimation is 1:10. Therefore estimated magnitude is slightly less than the existing one.

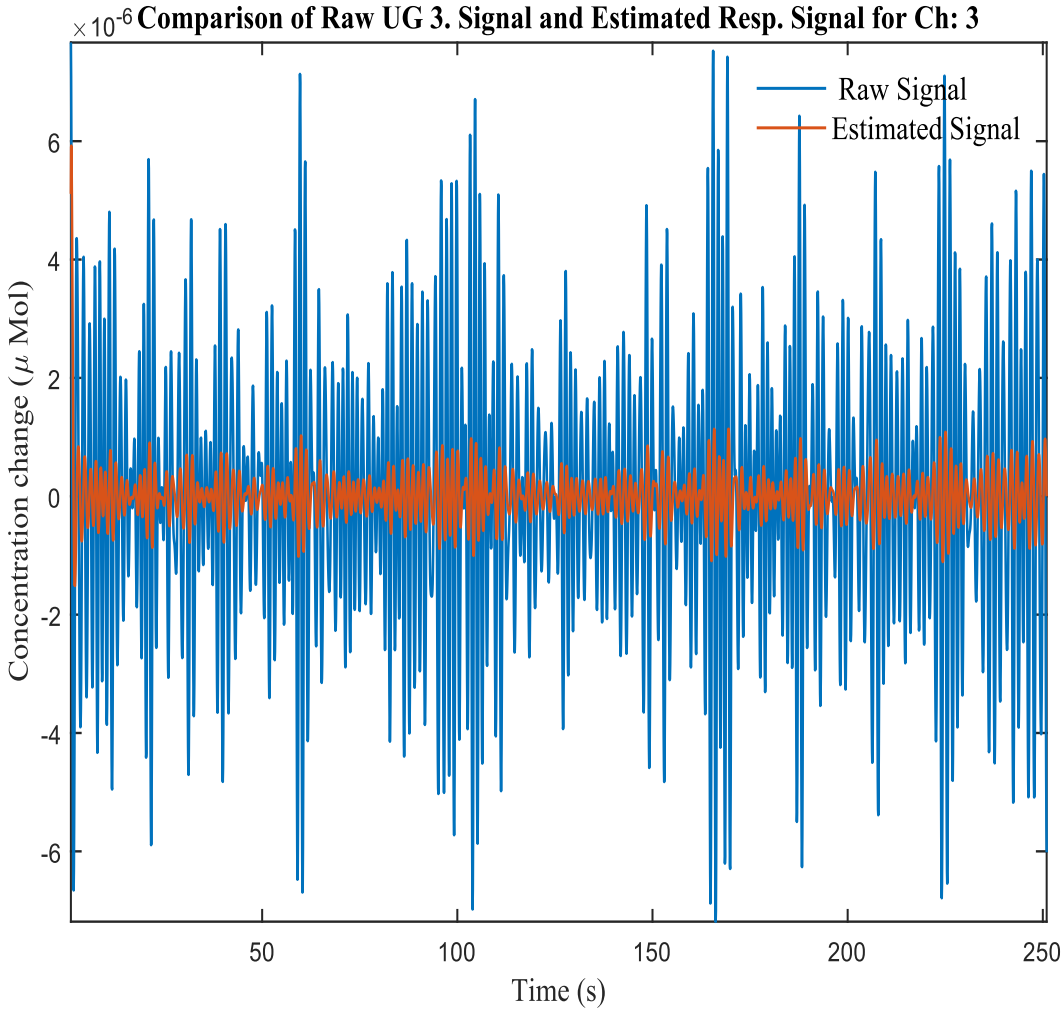

Figure 14: UG.3 signal before KF (blue) after KF (orange)

In **Figure: 14** it can be observed that before undergoing the process of Kalman estimation UG 3 signal has different magnitude. Kalman filter estimates the magnitude keeping account of the presence of measurement and process noise that can create or cause uneven increase or decrease in the magnitude of the signal. Ratio of process noise to measurement noise used in the estimation is 1:10. Therefore magnitude estimated is very less than the original one.

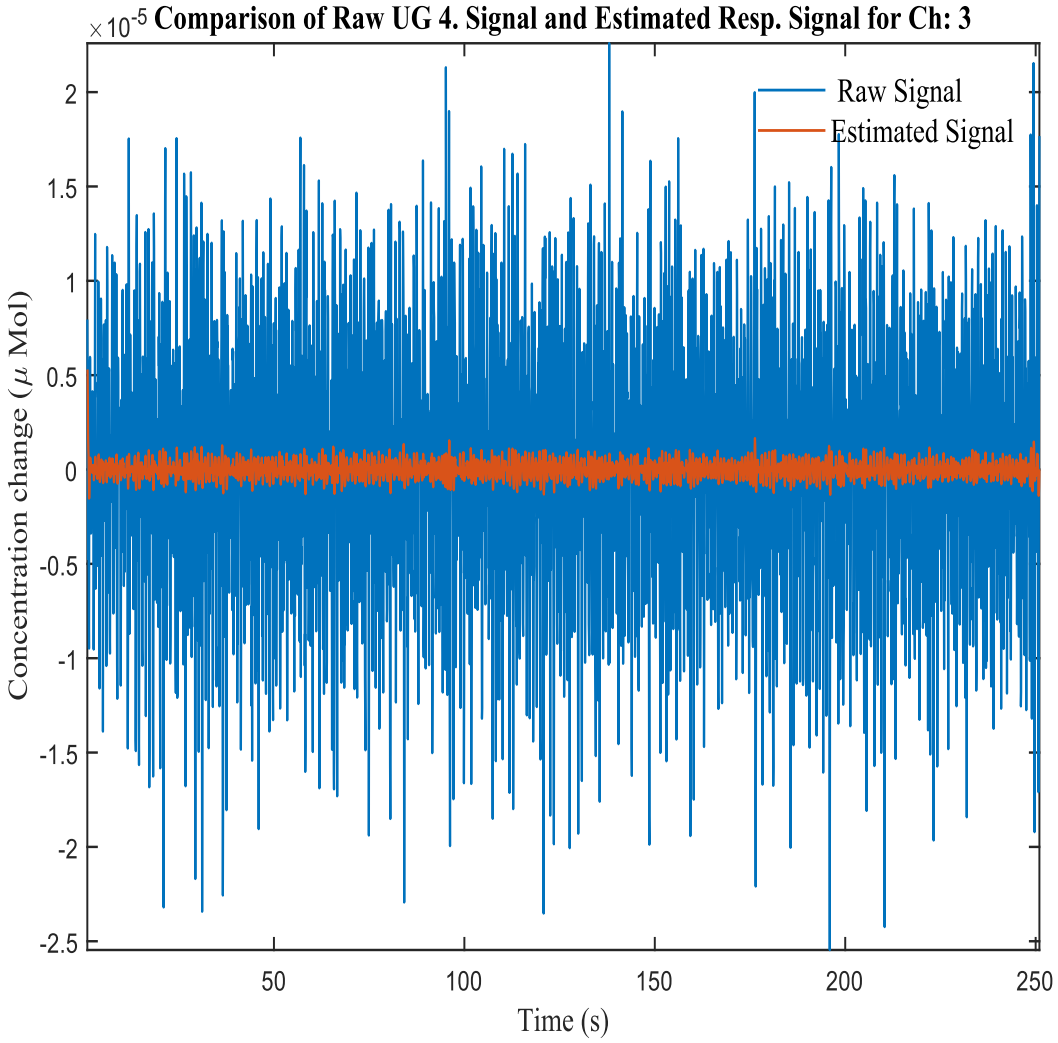

Figure 15: UG.4 signal before KF (blue) after KF (orange)

In **Figure: 15** it can be observed that before undergoing the process of Kalman estimation UG 4 signal has different magnitude. Kalman filter estimates the magnitude keeping account of the presence of measurement and process noise that can create or cause uneven increase or decrease in the magnitude of the signal. Ratio of process noise to measurement noise used in the estimation is 1:10. Therefore, estimated magnitude is very less than the original one.

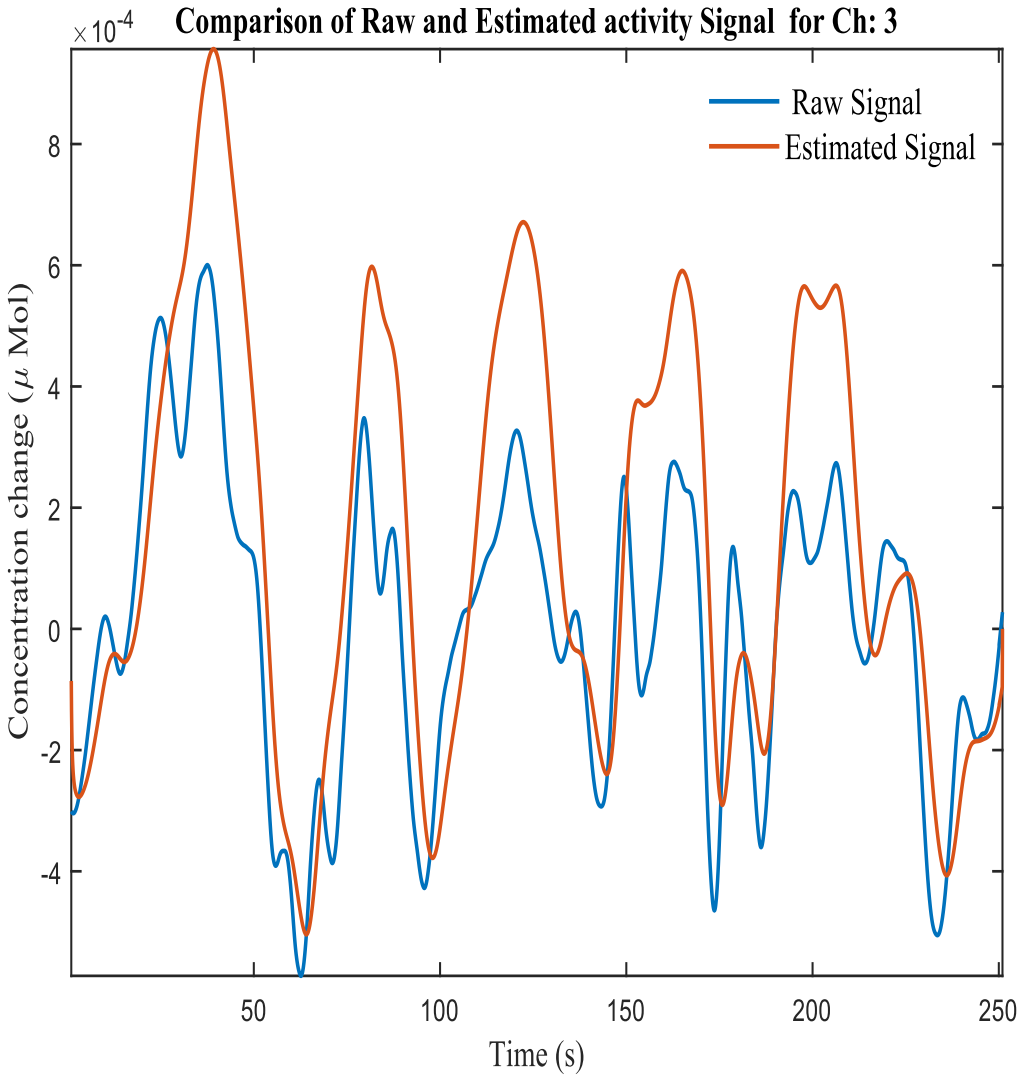

Figure 16: Activity signal before KF (blue) and after KF (orange)

In **Figure: 16** blue signal is the sum of details from level 7 to level 10 from discrete wavelet transform. Kalman filter estimates its magnitude based on the cHRF given as input.

4.4 Results from GLM

Wk- GLM is wavelet transform and Kalman filter based GLM. Following are the results of GLM for four active channels i.e., 3 , 10, 11 and 12.

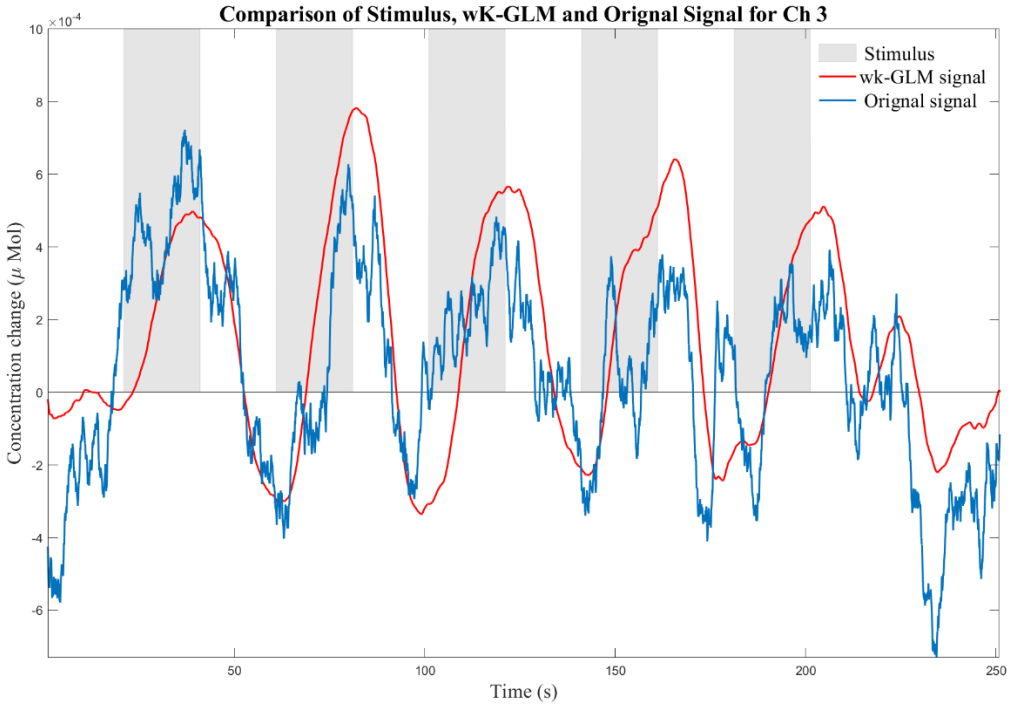

Figure 17: Results of wk GLM and Original signal for CH 3

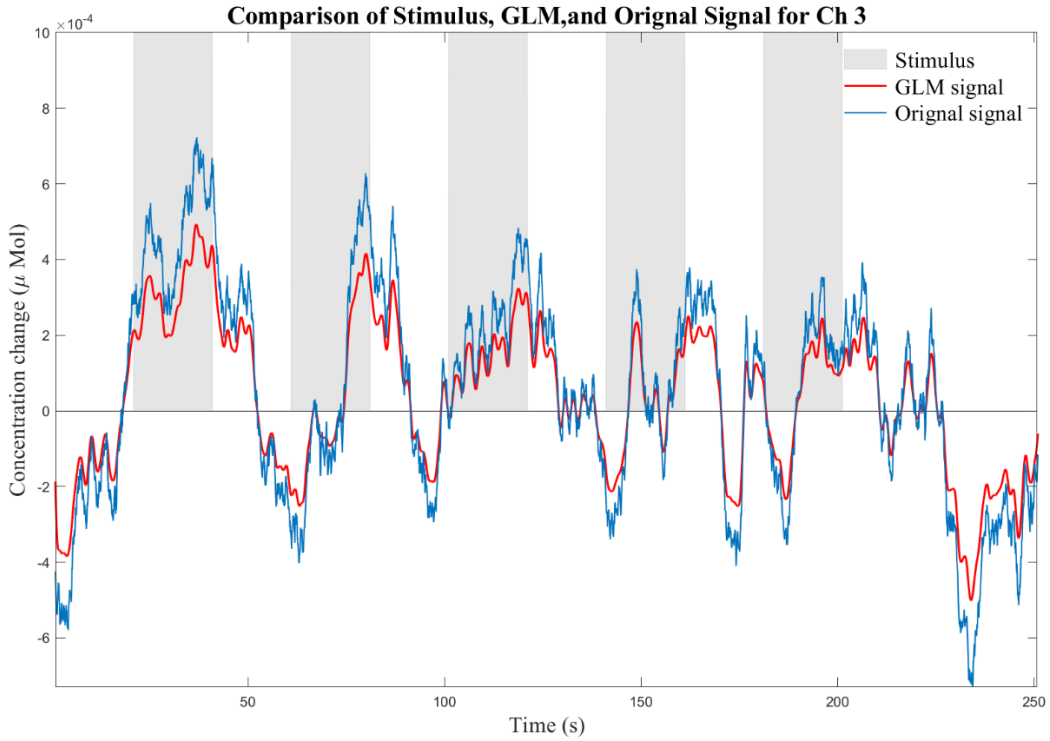

Figure 18:Results of GLM for CH 3

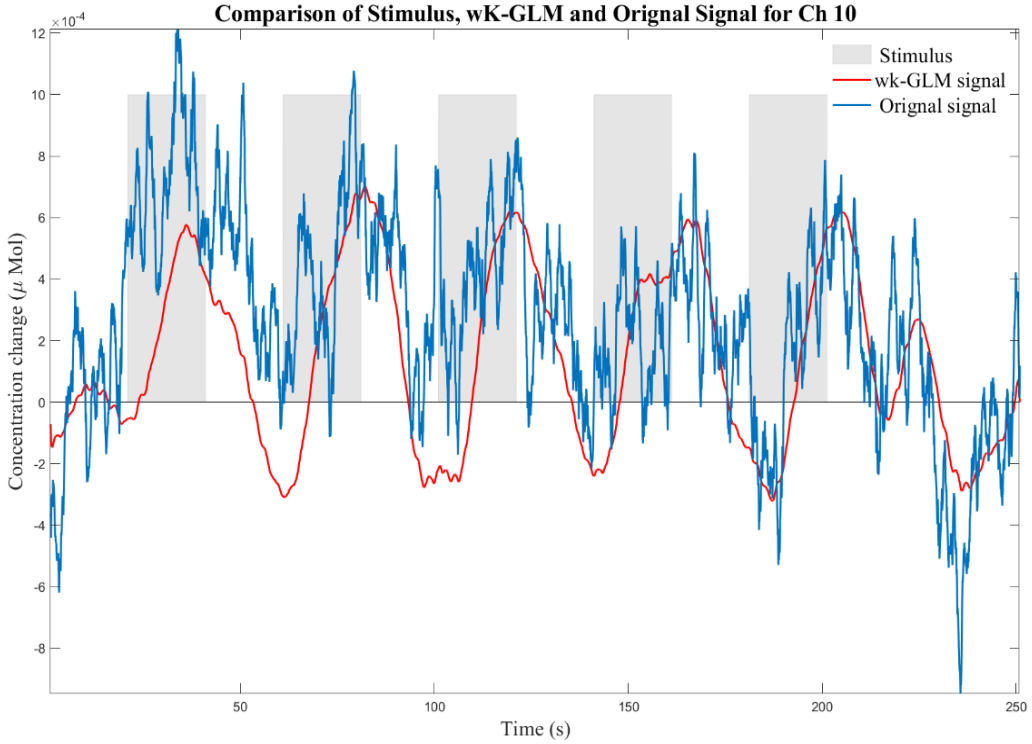

Figure 19:Results of wk GLM and Original signal for CH 10

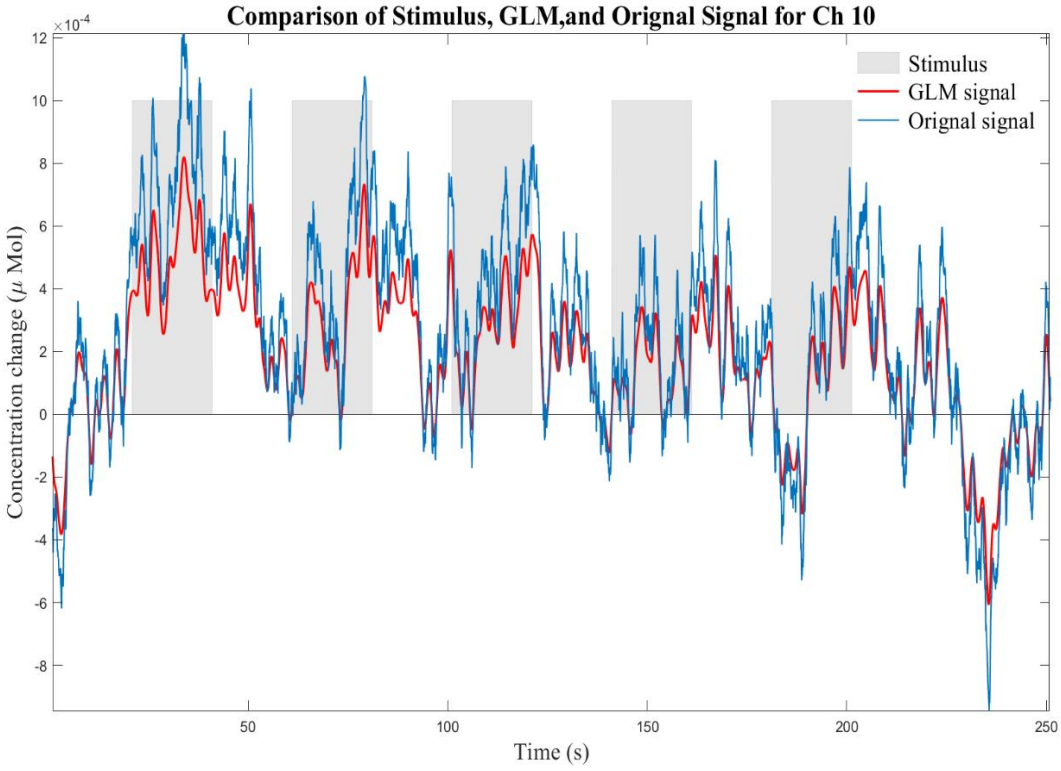

Figure 20:Results of wk GLM and GLM for CH 10

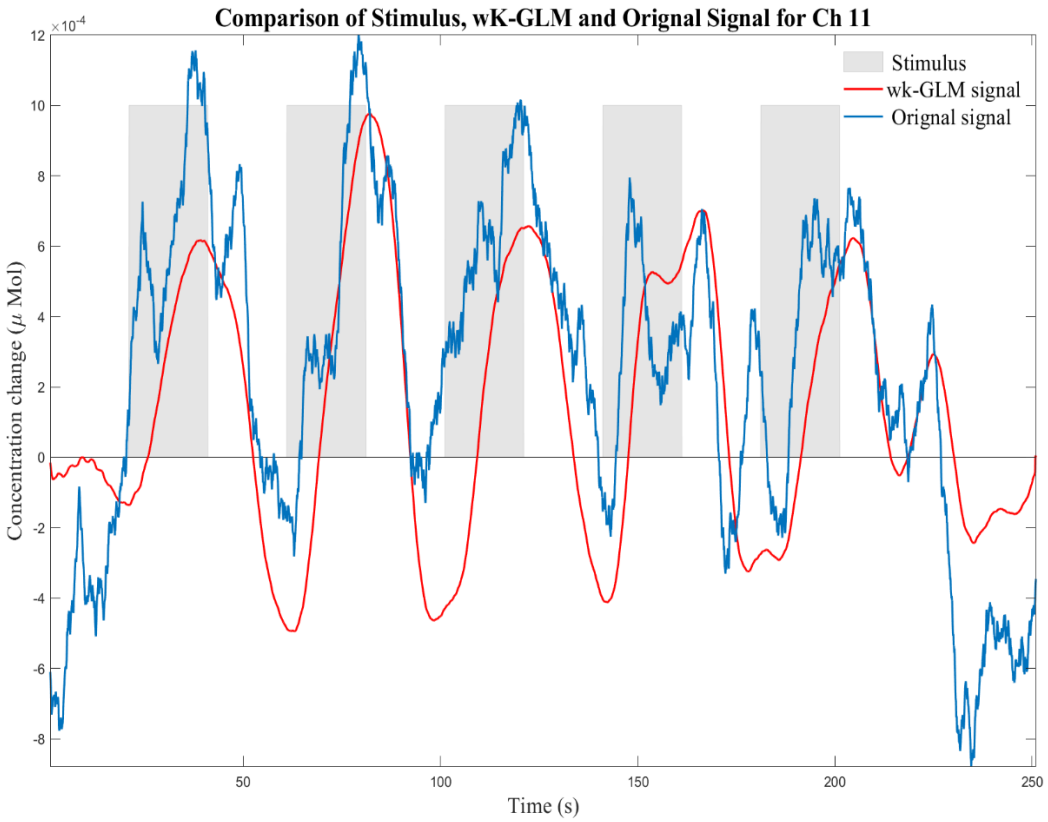

Figure 21:Results of wk GLM and Original Signal for CH 11

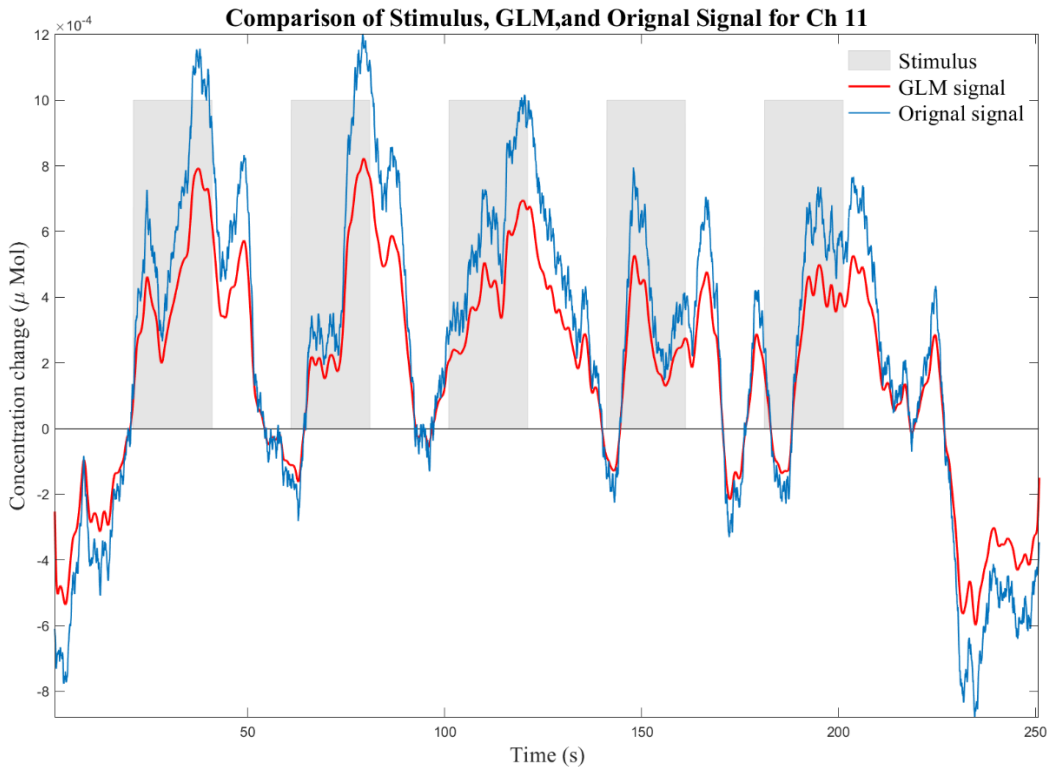

Figure 22: Result of GLM and Original Signal for CH 11

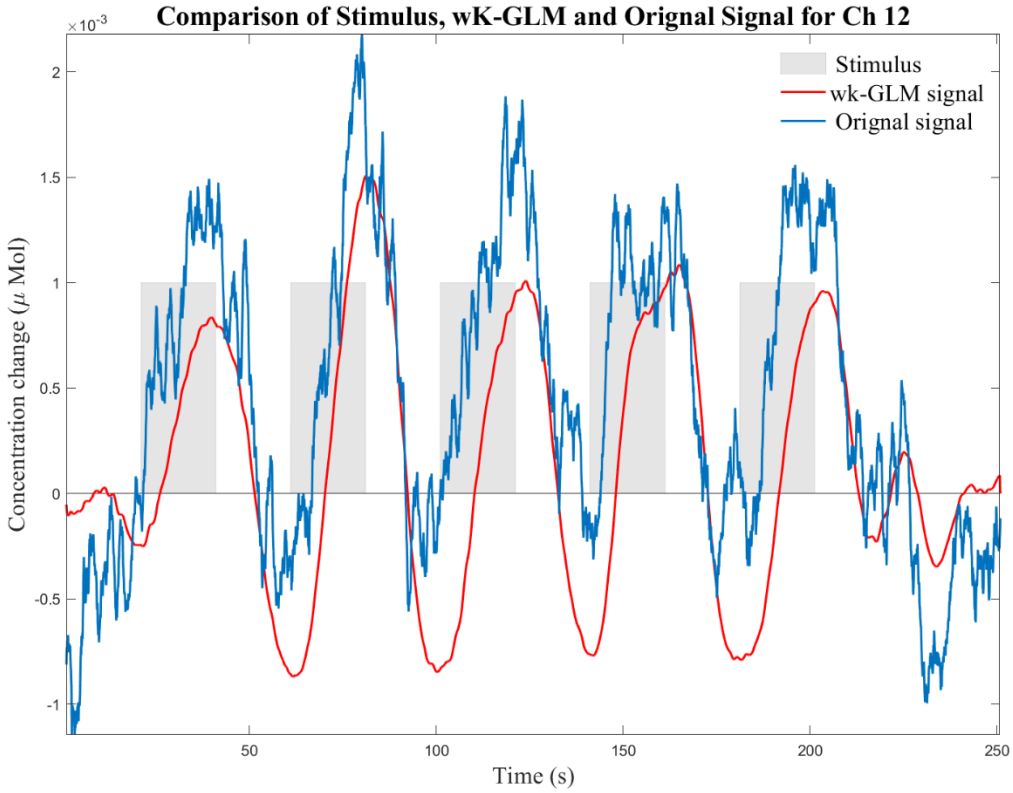

Figure 23: Result of wk-GLM and Original Signal for CH 12

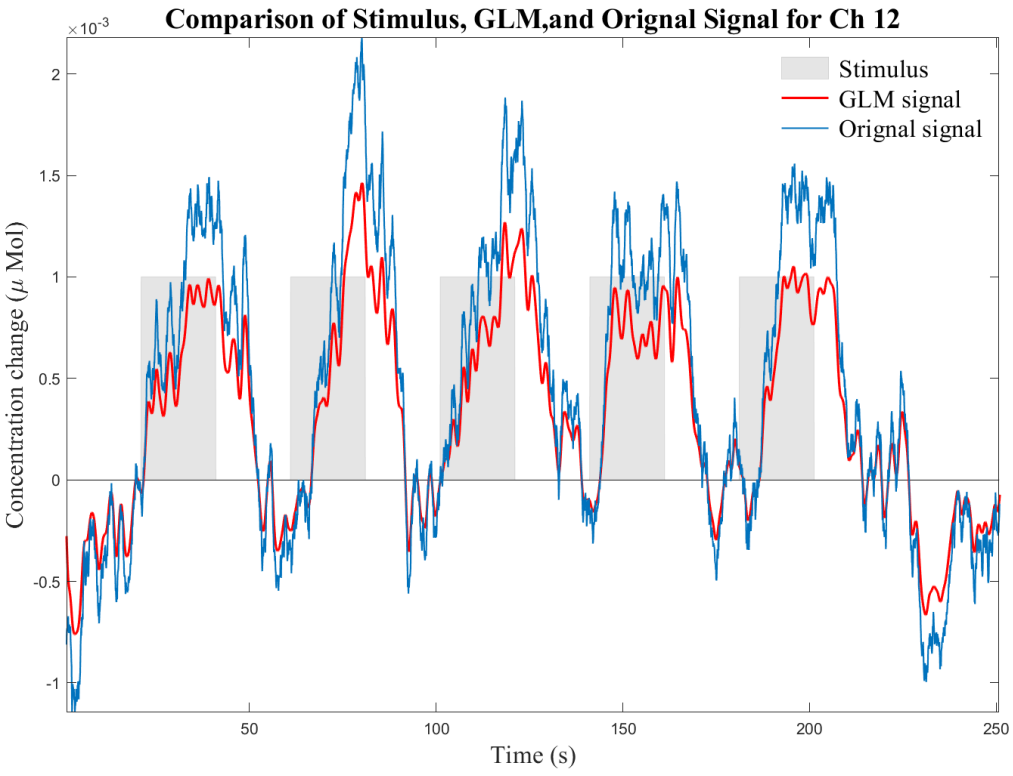

Figure 24: Result of GLM and Original Signal for CH 12

It is evident from the results that wavelet transform and Kalman filter based GLM (wk-GLM) yields results; smooth and close to canonical hemodynamic response function as compared to conventional GLM .

4.5 Brain activation maps for WK- GLM

After applying wavelet transform and Kalman filter based GLM brain activation maps are made for estimated signals. Results for Subject 3 are shown below.

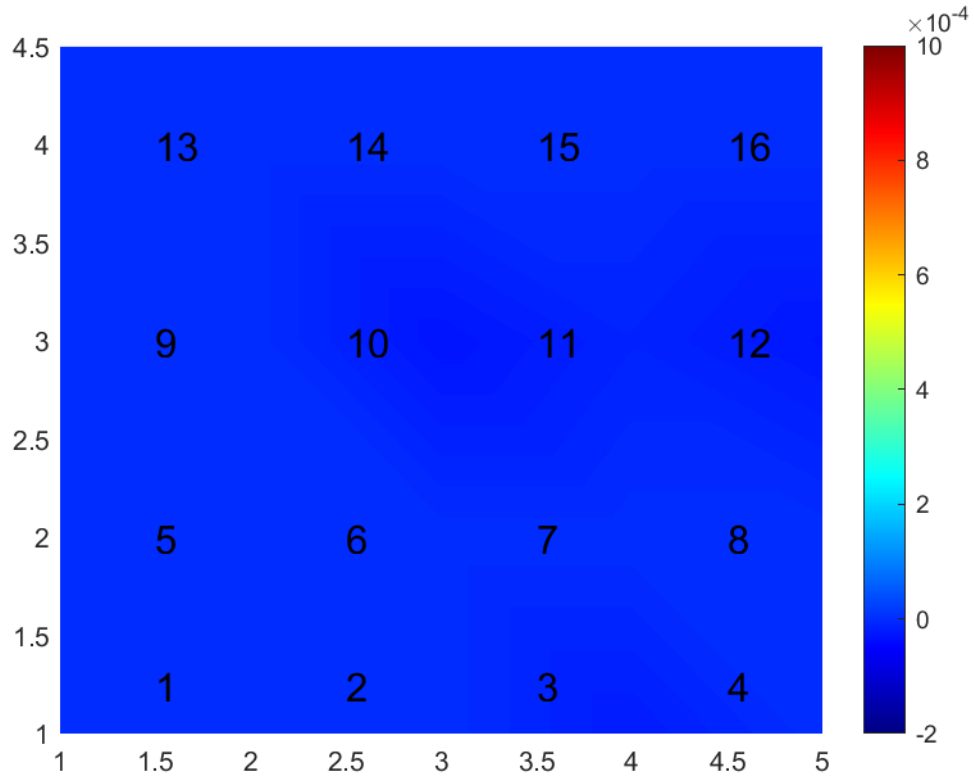

Figure 25:Activation map at 1 second

In **Figure: 25** no activation is observed as subject was doing rest.

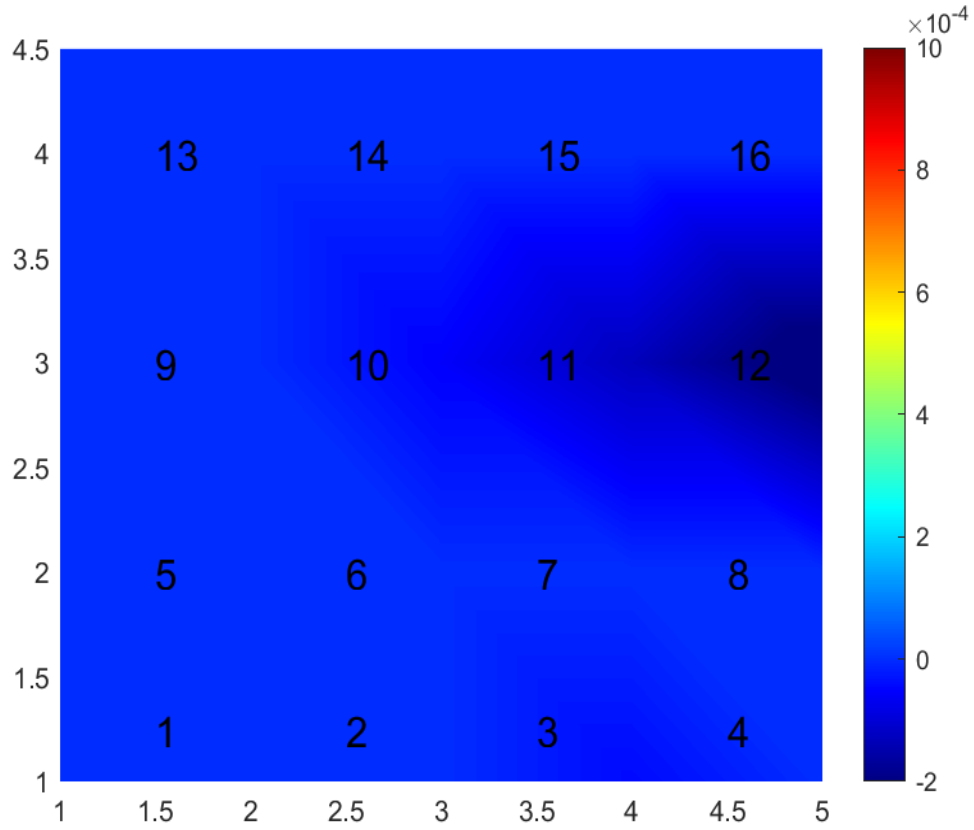

Figure 26:Activation map at 18 second

In **Figure: 26** dark blue shade can be observed around channel 11 and 12. This dark blue shade depicts initial dip.

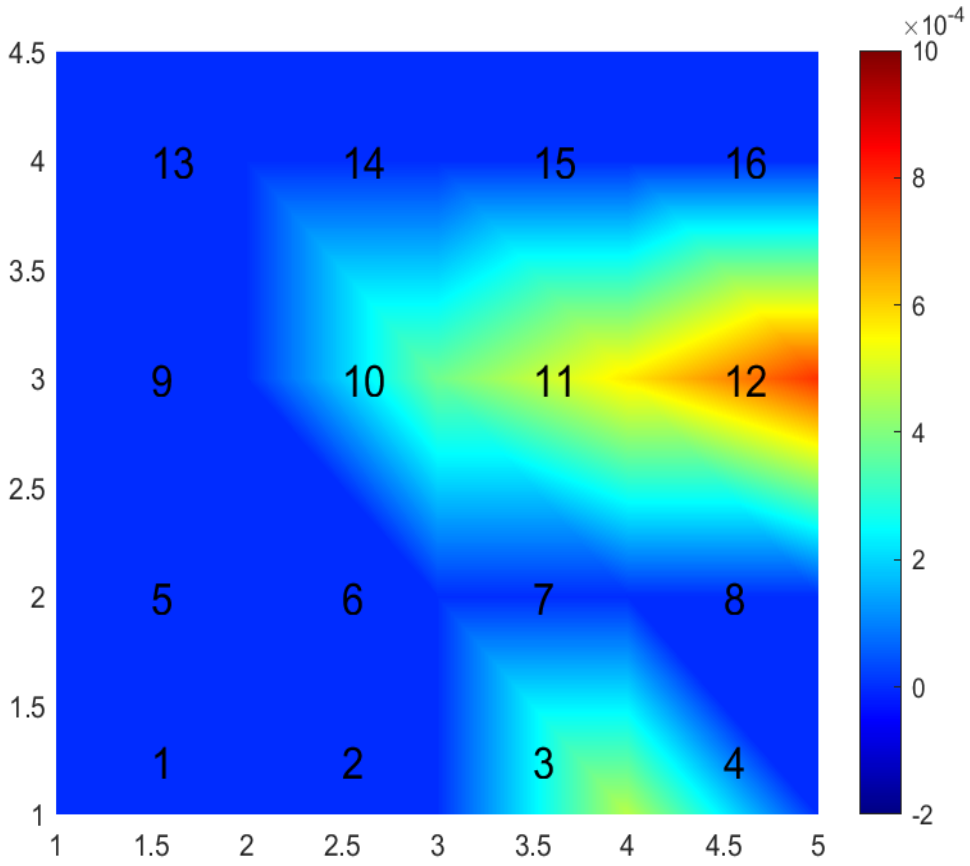

Figure 27: Activation map at 30 seconds

In **Figure: 27** yellowish red shade can be observed around channel 3, 10, 11, and 12 showing that activity is happening and increase in HbO can be observed.

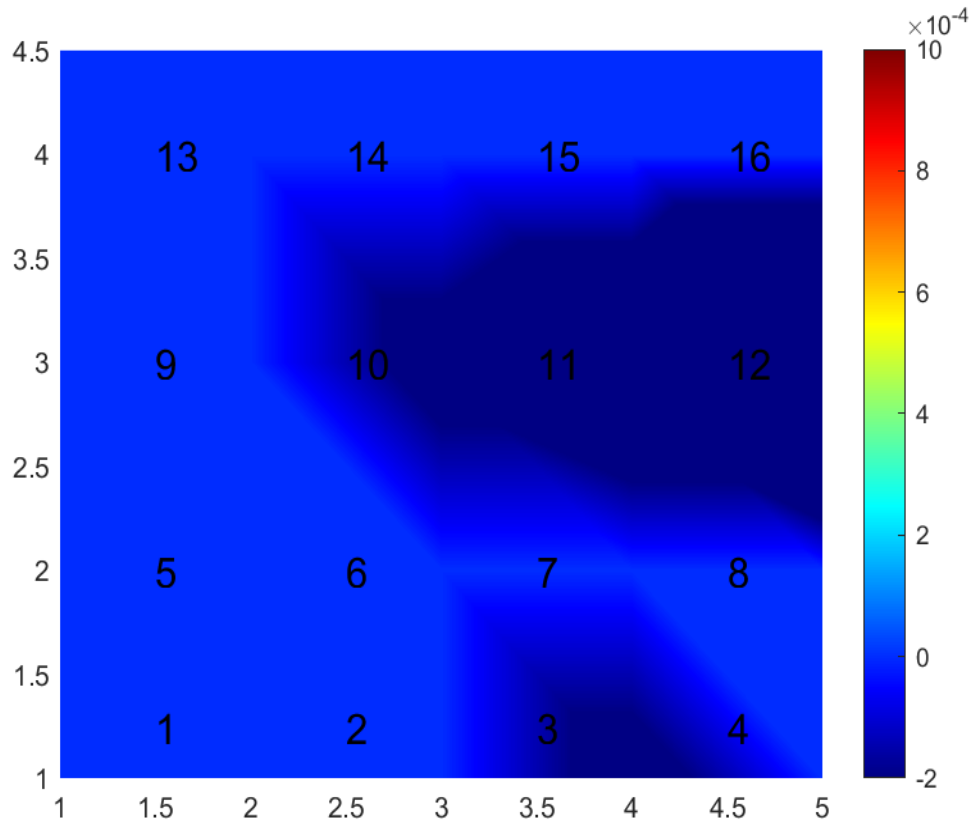

Figure 28:Activation map at 45 second

In **Figure: 28** it can be seen that at the end of activity or task dark blue shade has appeared again, this shows that signal is now below the zero level and HbR has started to increase.

4.6 Brain activation maps for GLM

Brain activation maps for already existing GLM method are shown under this section. Results for Subject 3 for finger tapping are shown below.

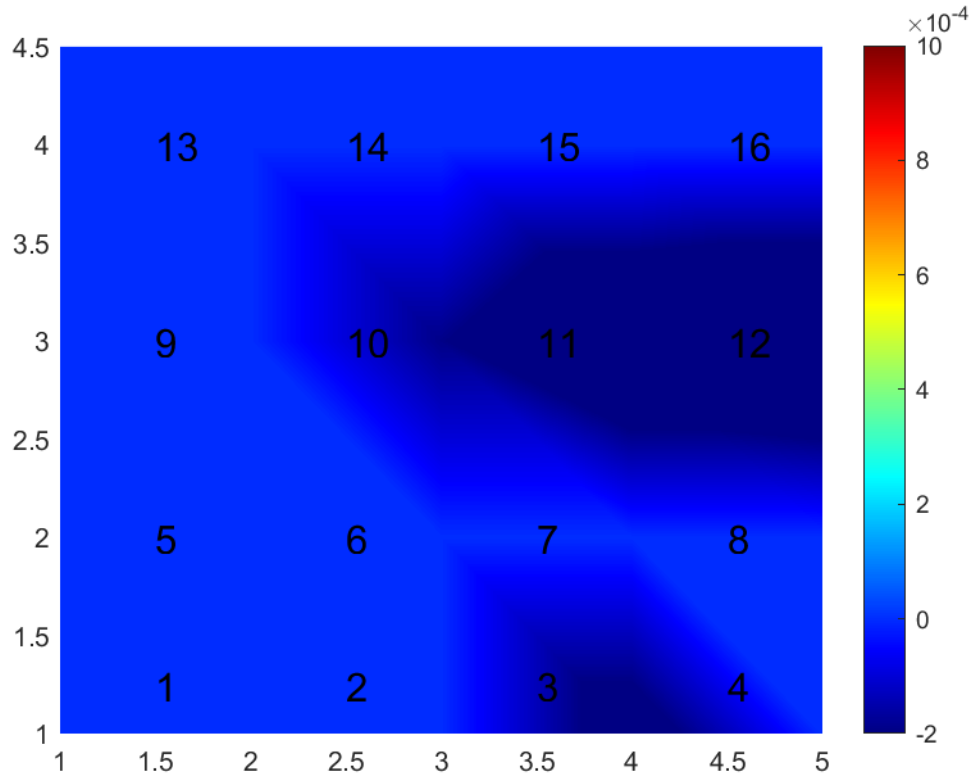

Figure 29: Activation map for GLM at 1st second

In **Figure: 29** above activation map for subject 3 at 1st second is shown. It can be seen that channel 3, 10, 11, and 12 have dark blue shade around them. This shade theoretically tells the limited supply of oxygen in that brain area. This should not be there because at 1st second subject was in resting state and stayed resting till 20th second.

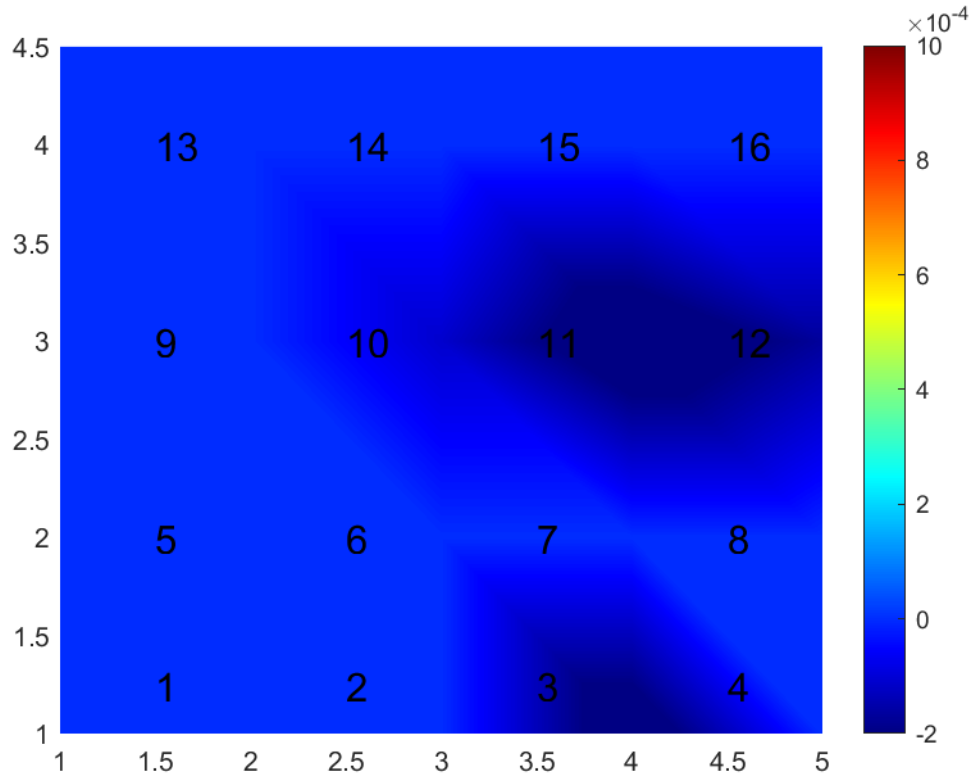

Figure 30: Activation map for GLM at 18th second

In **Figure: 30** activation map using GLM for subject 3 is shown. Dark blue shade depicts initial dip but in **Figure: 29** dark blue shade was already present even at 1st second when the subject was in resting state.

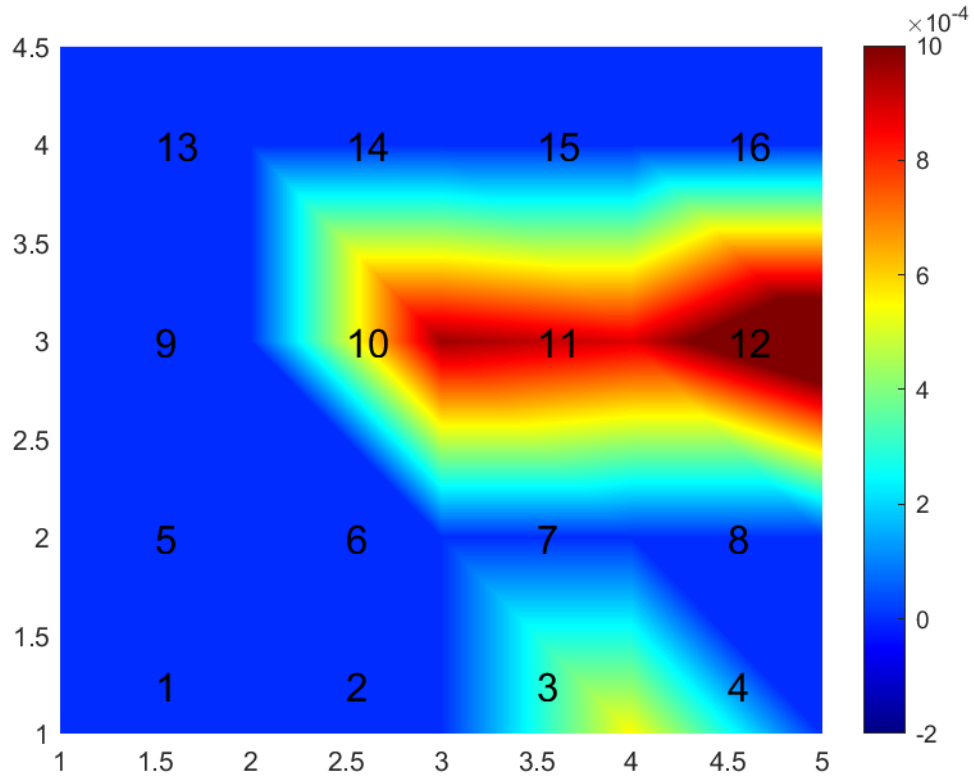

Figure 31: Activation map for GLM at 30th second

In **Figure: 31** it can be seen that all four channels are active and extra dark red shows higher magnitude for HbO . This can be due to over estimation of magnitude because of presence of noise.

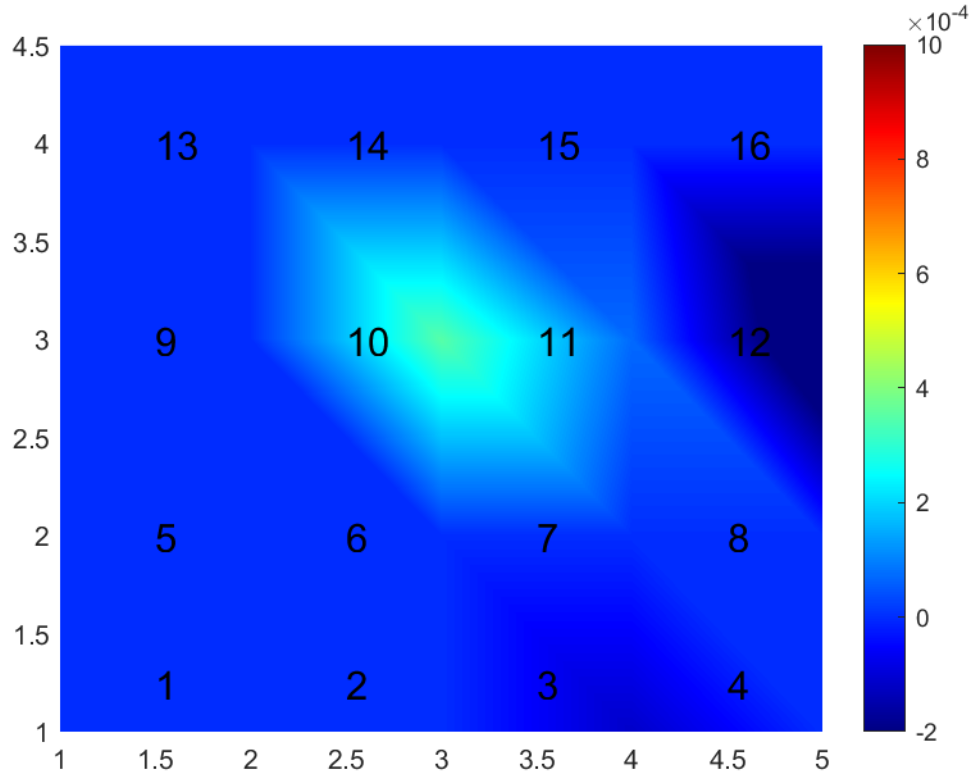

Figure 32 : Activation map for GLM at 45th second

In **Figure: 32** activation map for 45th second has been shown. It can be seen that channel 3 and 12 have dark blue shade which means that both of them have gone below the baseline. This behavior is understandable because the resting period has been started till this point. Channel 10 is still lit up and this means that signal at this channel has not returned to the baseline. It has drifted away from the baseline.

4.7 Statistical Significance

Following table shows the comparison between the t-values and signal to noise ratio (SNR) between wk-GLM and normal GLM method for subject 3.

Channel no	t-value for wk-GLM	t-value for GLM	SNR for wk-GLM (dB)	SNR for GLM (dB)
3	28.39	45.72	54.00	6.58
10	27.426	15.93	18.51	1.25
11	36.26	25.24	53.86	12.03
12	46.25	17.21	49.76	10.45

Table 1: t-values and SNR for subject 3

Channel no	t-value for wk-GLM	t-value for GLM	SNR for wk-GLM (dB)	SNR for GLM (dB)
3	23.92	16.25	34.85	6..05
10	25.21	13.42	30.62	9.21
11	31.54	17.70	35.86	12.76
12	39.46	19.35	37.18	9.83

Table 2: *t*-values and SNR for subject 1

From the tables it is evident that proposed method is better than the existing method. Only t-value for channel 3 of wk-GLM is less than the that of GLM. Values of SNR are also better than those acquired from conventional GLM.

Chapter 5: Conclusion & Future work

5.1 Conclusion

After observing the results of wavelet transform and Kalman filter based GLM different conclusions are drawn.

In proposed study, it has been observed that incorporating a range of noises compared to taking single discrete values yields results closer to cHRF. Frequency for physiological noises varies from person to person and rate of activity that is being performed. Using only single discrete value can cause over or under estimation of HRF signal. Moreover, taking a range of frequencies and modeling each noise helps in better understanding and reconstruction of real fNIRS signal. It also helps in adaptive estimation of signal as frequency are being varied in that range and thus, required signal of specific frequency at a particular time can be estimated.

This will help in the formation of more statistically correct brain activation maps which in turn aid in the fields of BCI ,BMI and brain disease diagnosis.

5.2 Future work

In brain computer interface at least six electrodes are required to make an interface. Size of each electrode is quite big. Moreover, after some time the neuronal path formed by the communication between neuron dies out. Since commands are executed on the basis of region of activation thus these two problems can lead to inaccurate communication between computer and brain. In such a case proposed method can be tested by using it along with BCI to locate the exact area for the activation of brain precisely.

In the past decade a rapid increase in the application of machine learning has been observed. There is not even a single field where machine learning is not involved. Machine learning works at its best when the data being used for training the algorithm is in refined form. Therefore, proposed study can be used along with ML algorithms in

refining the training data for fNIRS studies, and results can be compared with existing preprocessing techniques.

Claiming this work to be complete in all aspects will be misguiding. There is always room for improvement. The same process can be implemented using Unscented Kalman filters and particle filters.

Appendix

Loading the data

```
load('E:\Datasets\Authentic\RIFT_Imagent\RIFT_Imagent\FINGER TAP3.mat')
for i = 1:16
   oxy_sig(:,i) = nirs_data.oxyData (:,i);
end
oxy_sig = oxy_sig';
ch_no = input('Please enter the channel no = ')
siga = (oxy_sig(ch_no,:));
fs = 15.625; Q = 0.01; R = 25;
sig_1 = siga;
```

Setting up time axis

```
time = 1:1/fs:length(siga)/fs;
t = length(siga)-length(time);
t_frag = [time(end,end), zeros(1,t-1)];
for i =1:t-1
    t_frag(:,i+1) = t_frag(:,i) + 1/fs;
end
time = [time,t_frag];
```

Making cHRF

```
Parameters = [-0.2 10 -3.6 1.5 6.6 15 0.8 0.8 1];
hrf1 = threegamma(Parameters, [0:1/15.625:30]);
Stim_sig = nirs_data.vector_onset';
hrf_convolved_with_stim = (conv(Stim_sig,(hrf1)));
hcs = 0.9375e-4.*hrf_convolved_with_stim(1:length(siga));
```

Separation of signals

```
for j = 1:16
   sig_1 = oxy_sig(j,:)

% F = Fc/s*delta, where F = equivalent frequency, Fc = center frequency,
% s = scale and delta = sampling interval
[wt F] = cwt(siga,fs);
% for cardiac waves
FRQ.C = F; nc = 0;
%for respiratory waves
FRQ.R = F; nr = 0;
% for mayer waves
FRQ.M = F; nm = 0;
% for the remaining unknown frequencies bleow 0.1 hz
FRQ.U1 = F; nu1 = 0;
% for the frequencies between 0.1 hz and 0.3 hz
FRQ.U2 = F; nu2 = 0;
% for the frequencies between 0.3 hz and 0.6 hz
FRQ.U3 = F; nu3 = 0;
% for the frequencies between 0.1 hz and 0.3 hz
FRQ.U4 = F; nu4 = 0;
```

Separation and reconstruction of cardiac signal

```
for i = 1:length(FRQ.C)
   if (FRQ.C(i,1) > 0.7999)&(FRQ.C(i,1) < 1.2001)
      FRQ.C(i,1) = 1;
   else FRQ.C(i,1) = 0;
   end
end

for i = 1:length(F(:,1))
    if FRQ.C(i,1)==1
```

```
        Fr.card (i,:) = F(i,:);
    else
        Fr.card (i,:) = 0;
    end
end
Fr.card = nonzeros(Fr.card);
Fr.card = reshape(Fr.card,[],1);

for i = 1:length(FRQ.C)
   if FRQ.C(i,1)==1
      nc = nc+1;
   end
end

for i = 1:length(FRQ.C)
   if FRQ.C(i,1)==1
      new_wtc(i,:) = wt(i,:);
   else
      new_wtc(i,:) = zeros(1,length(wt(i,:)));
   end
end

rec.ca = icwt(new_wtc);
```

Separation and reconstruction of respiratory signal

```
for i = 1:length(FRQ.R)
   if (FRQ.R(i,1) > 0.2999)&(FRQ.R(i,1) < 0.6001)
      FRQ.R(i,1) = 1;
   else FRQ.R(i,1) = 0;
   end
end

for i = 1:length(F(:,1))
```

```
    if FRQ.R(i,1)==1
        Fr.resp (i,:) = F(i,:);
    else
        Fr.resp (i,:) = 0;
    end
end
Fr.resp = nonzeros(Fr.resp);
Fr.resp = reshape(Fr.resp,[],1);

for i = 1:length(FRQ.R)
   if FRQ.R(i,1)==1
      nr = nr+1;
   end
end

for i = 1:length(FRQ.R)
   if FRQ.R(i,1)==1
      new_wtr(i,:) = wt(i,:);
   else
      new_wtr(i,:) = zeros(1,length(wt(i,:)));
   end
end

rec.re = icwt(new_wtr);

%% Separation and reconstruction of mayer waves signal

for i = 1:length(FRQ.M)
   if (FRQ.M(i,1) > 0.09)&(FRQ.M(i,1) < 0.104)
      FRQ.M(i,1) = 1;
   else FRQ.M(i,1) = 0;
   end
end
```

```
for i = 1:length(F(:,1))
    if FRQ.M(i,1)==1
        Fr.mayer (i,:) = F(i,:);
    else
        Fr.mayer (i,:) = 0;
    end
end
Fr.mayer = nonzeros(Fr.mayer);
Fr.mayer = reshape(Fr.mayer,[],1);

for i = 1:length(FRQ.M)
   if FRQ.M(i,1)==1
      nm = nm+1;
   end
end

for i = 1:length(FRQ.M)
   if FRQ.M(i,1)==1
      new_wtm(i,:) = wt(i,:);
   else
      new_wtm(i,:) = zeros(1,length(wt(i,:)));
   end
end

rec.m = icwt(new_wtm);

%% Frequencies less than 0.1 hz

for i = 1:length(FRQ.U1)
   if (FRQ.U1(i,1) < 0.09)
      FRQ.U1(i,1) = 1;
   else FRQ.U1(i,1) = 0;
   end
end
```

```
for i = 1:length(F(:,1))
    if FRQ.U1(i,1)==1
        Fr.U1 (i,:) = F(i,:);
    else
        Fr.U1 (i,:) = 0;
    end
end
Fr.U1 = nonzeros(Fr.U1);
Fr.U1 = reshape(Fr.U1,[],1);

for i = 1:length(FRQ.U1)
   if FRQ.U1(i,1)==1
      nu1 = nu1+1;
   end
end

for i = 1:length(FRQ.U1)
   if FRQ.U1(i,1)==1
      new_wtu1(i,:) = wt(i,:);
   else
      new_wtu1(i,:) = zeros(1,length(wt(i,:)));
   end
end

rec.u1 = icwt(new_wtu1);

%% Frequencies above 0.1 hz and below 0.3 hz

for i = 1:length(FRQ.U2)
   if (FRQ.U2(i,1) > 0.1)&(FRQ.U2(i,1) < 0.3)
      FRQ.U2(i,1) = 1;
   else FRQ.U2(i,1) = 0;
   end
```

```
end

for i = 1:length(F(:,1))
    if FRQ.U2(i,1)==1
        Fr.U2 (i,:) = F(i,:);
    else
        Fr.U2 (i,:) = 0;
    end
end
Fr.U2 = nonzeros(Fr.U2);
Fr.U2 = reshape(Fr.U2,[],1);

for i = 1:length(FRQ.U2)
   if FRQ.U2(i,1)==1
       nu2 = nu2+1;
   end
end

for i = 1:length(FRQ.U2)
   if FRQ.U2(i,1)==1
       new_wtu2(i,:) = wt(i,:);
   else
       new_wtu2(i,:) = zeros(1,length(wt(i,:)));
   end
end

rec.u2 = icwt(new_wtu2);

%% Frequencies between 0.6 hz and 0.79 hz

for i = 1:length(FRQ.U3)
   if (FRQ.U3(i,1) > 0.6)&(FRQ.U3(i,1) < 0.8)
       FRQ.U3(i,1) = 1;
   else FRQ.U3(i,1) = 0;
```

```
    end
end

for i = 1:length(F(:,1))
    if FRQ.U3(i,1)==1
        Fr.U3 (i,:) = F(i,:);
    else
        Fr.U3 (i,:) = 0;
    end
end
Fr.U3 = nonzeros(Fr.U3);
Fr.U3 = reshape(Fr.U3,[],1);

for i = 1:length(FRQ.U3)
    if FRQ.U3(i,1)==1
        nu3 = nu3+1;
    end
end

for i = 1:length(FRQ.U3)
    if FRQ.U3(i,1)==1
        new_wtu3(i,:) = wt(i,:);
    else
        new_wtu3(i,:) = zeros(1,length(wt(i,:)));
    end
end

rec.u3 = icwt(new_wtu3);
%% Frequencies above 1.2 hz

for i = 1:length(FRQ.U4)
    if (FRQ.U4(i,1) > 1.2)
        FRQ.U4(i,1) = 1;
    else FRQ.U4(i,1) = 0;
```

```
    end
end

for i = 1:length(F(:,1))
    if FRQ.U4(i,1)==1
        Fr.U4 (i,:) = F(i,:);
    else
        Fr.U4 (i,:) = 0;
    end
end
Fr.U4 = nonzeros(Fr.U4);
Fr.U4 = reshape(Fr.U4,[],1);

for i = 1:length(FRQ.U4)
    if FRQ.U4(i,1)==1
        nu4 = nu4+1;
    end
end

for i = 1:length(FRQ.U4)
    if FRQ.U4(i,1)==1
        new_wtu4(i,:) = wt(i,:);
    else
        new_wtu4(i,:) = zeros(1,length(wt(i,:)));
    end
end

rec.u4 = icwt(new_wtu4);
% recon ={rec.ca;rec.re;rec.m;rec.u1;rec.u2;rec.u3;rec.u4};
rc(:,j) ={rec.ca;rec.re;rec.m;rec.u1;rec.u2;rec.u3;rec.u4};

end
```

Creating back signal for every single frequency

```
for i= 1 : length(wt(:,1))

   f_sig(i,:) = icwt([wt(i,:);zeros(1,length(wt(1,:)))]);

end
```

Separating the reconstructed cardiac signals.

```
for i= 1:length(f_sig(:,1))
   if FRQ.C(i,:)==1
      mat.card(i,:)=f_sig(i,:);
   else
      null.card(i,:) = zeros(1,length(f_sig(1,:)));
   end
end

mat.card_new = nonzeros(mat.card);
mat.card_new = reshape(mat.card_new,[],length(f_sig(1,:)));
```

Separating the reconstructed respiratory signals.

```
for i= 1:length(f_sig(:,1))
   if FRQ.R(i,:)==1
      mat.resp(i,:)=f_sig(i,:);
   else
      null.resp(i,:) = zeros(1,length(f_sig(1,:)));
   end
end

mat.resp_new = nonzeros(mat.resp);
mat.resp_new = reshape(mat.resp_new,[],length(f_sig(1,:)));
```

Separating the reconstructed mayer signals.

```
for i= 1:length(f_sig(:,1))
   if FRQ.M(i,:)==1
      mat.mayer(i,:)=f_sig(i,:);
   else
      null.mayer(i,:) = zeros(1,length(f_sig(1,:)));
   end
end

mat.mayer_new = nonzeros(mat.mayer);
mat.mayer_new = reshape(mat.mayer_new,[],length(f_sig(1,:)));
```

Separating the reconstructed Unknown signals Group 1 (F < 0.1 hz)

```
for i= 1:length(f_sig(:,1))
   if FRQ.U1(i,:)==1
      mat.U1(i,:)=f_sig(i,:);
   else
      null.U1(i,:) = zeros(1,length(f_sig(1,:)));
   end
end

mat.U1_new = nonzeros(mat.U1);
mat.U1_new = reshape(mat.U1_new,[],length(f_sig(1,:)));
```

Separating the reconstructed Unknown signals Group 2 (0.3 hz > F < 0.6 hz)

```
for i= 1:length(f_sig(:,1))
   if FRQ.U2(i,:)==1
      mat.U2(i,:)=f_sig(i,:);
   else
      null.U2(i,:) = zeros(1,length(f_sig(1,:)));
   end
end
```

```
mat.U2_new = nonzeros(mat.U2);
mat.U2_new = reshape(mat.U2_new,[],length(f_sig(1,:)));
```

Separating the reconstructed Unknown signals Group 3 (0.6 hz > F < 0.8 hz)

```
for i= 1:length(f_sig(:,1))
   if FRQ.U3(i,:)==1
      mat.U3(i,:)=f_sig(i,:);
   else
      null.U3(i,:) = zeros(1,length(f_sig(1,:)));
   end
end

mat.U3_new = nonzeros(mat.U3);
mat.U3_new = reshape(mat.U3_new,[],length(f_sig(1,:)));
```

Separating the reconstructed Unknown signals Group 4 (F > 1.2 hz)

```
for i= 1:length(f_sig(:,1))
   if FRQ.U4(i,:)==1
      mat.U4(i,:)=f_sig(i,:);
   else
      null.U4(i,:) = zeros(1,length(f_sig(1,:)));
   end
end

mat.U4_new = nonzeros(mat.U4);
mat.U4_new = reshape(mat.U4_new,[],length(f_sig(1,:)));
```

Generating magnitude of cardiac signals

```
for i = 1: length(Fr.card(:,1))
   freq.card(i,:) = sin(2*pi*Fr.card(i,:));
end

for i= 1:length(mat.card_new(:,1))
      mag_mat.card(i,:)=  mat.card_new(i,:)/freq.card(i,:);
end
```

Generating magnitude of respiratory signal

```
for i = 1: length(Fr.resp(:,1))
   freq.resp(i,:) = sin(2*pi*Fr.resp(i,:));
end

for i= 1:length(mat.resp_new(:,1))
      mag_mat.resp(i,:)=  mat.resp_new(i,:)/freq.resp(i,:);
end
```

Generating magnitude of mayer signal

```
for i = 1: length(Fr.mayer(:,1))
   freq.mayer(i,:) = sin(2*pi*Fr.mayer(i,:));
end

for i= 1:length(mat.mayer_new(:,1))
      mag_mat.mayer(i,:)=  mat.mayer_new(i,:)/freq.mayer(i,:);
end
```

Generating magnitude of Unknown signal group 1

```
for i = 1: length(Fr.U1(:,1))
   freq.U1(i,:) = sin(2*pi*Fr.U1(i,:));
```

```
end

for i= 1:length(mat.U1_new(:,1))
      mag_mat.U1(i,:)=  mat.U1_new(i,:)/freq.U1(i,:);
end
```

Generating magnitude of Unknown signal group 2

```
for i = 1: length(Fr.U2(:,1))
   freq.U2(i,:) = sin(2*pi*Fr.U2(i,:));
end

for i= 1:length(mat.U2_new(:,1))
      mag_mat.U2(i,:)=  mat.U2_new(i,:)/freq.U2(i,:);
end
```

Generating magnitude of Unknown signal group 3

```
for i = 1: length(Fr.U3(:,1))
   freq.U3(i,:) = sin(2*pi*Fr.U3(i,:));
end

for i= 1:length(mat.U3_new(:,1))
      mag_mat.U3(i,:)=  mat.U3_new(i,:)/freq.U3(i,:);
end
```

Generating magnitude of Unknown signal group 4

```
for i = 1: length(Fr.U4(:,1))
   freq.U4(i,:) = sin(2*pi*Fr.U4(i,:));
end
for i= 1:length(mat.U4_new(:,1))
      mag_mat.U4(i,:)=  mat.U4_new(i,:)/freq.U4(i,:);
end
```

Applying Kalman Filter

```
KG    =   zeros(1,length(sig_1));
EST   =   zeros(1,length(sig_1));
Eest  =   1e-4.*(ones(1,length(sig_1)));
Emea  =   0.25e-6.*(ones(1,length(sig_1)));
MEA   =   sig_1';

for i = 1:length(MEA)
   if i == 1
      KG(1,i)   = Eest/(Eest + Emea);
      EST(1,i)  = EST(1,i) + KG(1,i)*(MEA(1,i) - EST(1,i));
      Eest      = (1 - KG(1,i))*(Eest);
   else
      KG(1,i)   = (Eest)/(Eest + Emea);
      EST(1,i)  = (1-KG(1,i))*EST(1,i-1) + KG(1,i)*(MEA(1,i));
      Eest      = (1 - KG(1,i))*(Eest);
   end
end
```

Applying GLM

```
siga = oxy_sig(3,:);
sgnl = zeros(1,length(siga));

for j = 1:16

   sgnl = zeros(1,length(siga));

   for i = 1:3
      sgnl = sgnl + Kal_rc{i, j} ;
   end

   s_sig = sgnl;
```

```
    for b = 1:4

        h_rd = KE{b,j};
        g_sg(b,:) = h_rd+[diff(h_rd),0]+[diff(diff(h_rd)), 0,0]+s_sig;

    end

    clear b
    glm(:,j) ={g_sg(1,:);g_sg(2,:);g_sg(3,:);g_sg(4,:)};

    for b = 1:4
        err(b,:) = oxy_sig(b,:) - g_sg(b,:);
    end
    c_err(:,j) = {err(1,:),err(2,:),err(3,:),err(4,:)};
end
```

References

[1] A. Villringer and B. Chance, "Non-invasive optical spectroscopy and imaging of human brain function," *Trends Neurosci,* vol. 20, no. 10, pp. 435-42, Oct 1997.

[2] G. Gratton, M. R. Goodman-Wood, and M. Fabiani, "Comparison of neuronal and hemodynamic measures of the brain response to visual stimulation: an optical imaging study," *Hum Brain Mapp,* vol. 13, no. 1, pp. 13-25, May 2001.

[3] P. T. Fox, M. E. Raichle, M. A. Mintun, and C. Dence, "Nonoxidative glucose consumption during focal physiologic neural activity," *Science,* vol. 241, no. 4864, pp. 462-4, Jul 22 1988.

[4] H. Obrig and A. Villringer, "Beyond the visible--imaging the human brain with light," *J Cereb Blood Flow Metab,* vol. 23, no. 1, pp. 1-18, Jan 2003.

[5] S. Ogawa, T. M. Lee, A. R. Kay, and D. W. Tank, "Brain magnetic resonance imaging with contrast dependent on blood oxygenation," *Proc Natl Acad Sci U S A,* vol. 87, no. 24, pp. 9868-72, Dec 1990.

[6] B. Chance, Z. Zhuang, C. UnAh, C. Alter, and L. Lipton, "Cognition-activated low-frequency modulation of light absorption in human brain," *Proc Natl Acad Sci U S A,* vol. 90, no. 8, pp. 3770-4, Apr 15 1993.

[7] F. F. Jobsis, "Noninvasive, infrared monitoring of cerebral and myocardial oxygen sufficiency and circulatory parameters," *Science,* vol. 198, no. 4323, pp. 1264-7, Dec 23 1977.

[8] A. F. Abdelnour and T. Huppert, "Real-time imaging of human brain function by near-infrared spectroscopy using an adaptive general linear model," *Neuroimage,* vol. 46, no. 1, pp. 133-43, May 15 2009.

[9] H. Karim, B. Schmidt, D. Dart, N. Beluk, and T. Huppert, "Functional near-infrared spectroscopy (fNIRS) of brain function during active balancing using a video game system," *Gait Posture,* vol. 35, no. 3, pp. 367-72, Mar 2012.

[10] D. A. Boas, A. M. Dale, and M. A. Franceschini, "Diffuse optical imaging of brain activation: approaches to optimizing image sensitivity, resolution, and accuracy," *Neuroimage,* vol. 23 Suppl 1, pp. S275-88, 2004.

[11] H. Koizumi *et al.,* "Optical topography: practical problems and new applications," *Appl Opt,* vol. 42, no. 16, pp. 3054-62, Jun 1 2003.

[12] S. Perrey, "Non-invasive NIR spectroscopy of human brain function during exercise," *Methods,* vol. 45, no. 4, pp. 289-99, Aug 2008.

[13] X. S. Hu, K. S. Hong, S. S. Ge, and M. Y. Jeong, "Kalman estimator- and general linear model-based on-line brain activation mapping by near-infrared spectroscopy," *Biomed Eng Online,* vol. 9, p. 82, Dec 8 2010.

[14] F. Irani, S. M. Platek, S. Bunce, A. C. Ruocco, and D. Chute, "Functional near infrared spectroscopy (fNIRS): an emerging neuroimaging technology with important applications for the study of brain disorders," *Clin Neuropsychol,* vol. 21, no. 1, pp. 9-37, Jan 2007.

[15] V. Quaresima and M. Ferrari, "Functional Near-Infrared Spectroscopy (fNIRS) for Assessing Cerebral Cortex Function During Human Behavior in Natural/Social Situations: A Concise Review," vol. 22, no. 1, pp. 46-68, 2019.

[16] G. Gratton, J. S. Maier, M. Fabiani, W. W. Mantulin, and E. Gratton, "Feasibility of intracranial near-infrared optical scanning," *Psychophysiology,* vol. 31, no. 2, pp. 211-5, Mar 1994.

[17] W. B. Baker, A. B. Parthasarathy, D. R. Busch, R. C. Mesquita, J. H. Greenberg, and A. G. Yodh, "Modified Beer-Lambert law for blood flow," *Biomed Opt Express,* vol. 5, no. 11, pp. 4053-75, Nov 1 2014.

[18] M. R. Bhutta, K. S. Hong, B. M. Kim, M. J. Hong, Y. H. Kim, and S. H. Lee, "Note: three wavelengths near-infrared spectroscopy system for compensating the light absorbance by water," *Rev Sci Instrum,* vol. 85, no. 2, p. 026111, Feb 2014.

[19] N. D. Tam and G. Zouridakis, "Differential temporal activation of oxy-and deoxy-hemodynamic signals in optical imaging using functional near-infrared spectroscopy (fNIRS)," vol. 16, no. 1, pp. 1-2, 2015.

[20] X. S. Hu, K. S. Hong, and S. S. Ge, "fNIRS-based online deception decoding," *J Neural Eng,* vol. 9, no. 2, p. 026012, Apr 2012.

[21] F. Scholkmann *et al.*, "A review on continuous wave functional near-infrared spectroscopy and imaging instrumentation and methodology," *Neuroimage,* vol. 85 Pt 1, pp. 6-27, Jan 15 2014.

[22] P. Piaggi, D. Menicucci, C. Gentili, G. Handjaras, A. Gemignani, and A. Landi, "Singular spectrum analysis and adaptive filtering enhance the functional connectivity analysis of resting state fMRI data," vol. 24, no. 03, p. 1450010, 2014.

[23] M. J. Hofmann *et al.*, "Differential activation of frontal and parietal regions during visual word recognition: an optical topography study," *Neuroimage*, vol. 40, no. 3, pp. 1340-9, Apr 15 2008.

[24] V. Kaiser *et al.*, "Cortical effects of user training in a motor imagery based brain-computer interface measured by fNIRS and EEG," *Neuroimage*, vol. 85 Pt 1, pp. 432-44, Jan 15 2014.

[25] M. A. Yucel, J. Selb, R. J. Cooper, and D. A. Boas, "Targeted Principle Component Analysis: A New Motion Artifact Correction Approach for near-Infrared Spectroscopy," *J Innov Opt Health Sci*, vol. 7, no. 2, Mar 1 2014.

[26] P. W. Dans, S. D. Foglia, and A. J. Nelson, "Data Processing in Functional Near-Infrared Spectroscopy (fNIRS) Motor Control Research," *Brain Sci*, vol. 11, no. 5, May 9 2021.

[27] W. D. Penny, K. J. Friston, J. T. Ashburner, S. J. Kiebel, and T. E. Nichols, *Statistical parametric mapping: the analysis of functional brain images*. Elsevier, 2011.

[28] M. A. Kamran and K.-S. Hong, "Reduction of physiological effects in fNIRS waveforms for efficient brain-state decoding," vol. 580, pp. 130-136, 2014.

[29] G. Strangman, J. P. Culver, J. H. Thompson, and D. A. Boas, "A quantitative comparison of simultaneous BOLD fMRI and NIRS recordings during functional brain activation," vol. 17, no. 2, pp. 719-731, 2002.

[30] M. M. Plichta *et al.*, "Event-related functional near-infrared spectroscopy (fNIRS): are the measurements reliable?," vol. 31, no. 1, pp. 116-124, 2006.

[31] M. Plichta *et al.*, "Event-related functional near-infrared spectroscopy (fNIRS) based on craniocerebral correlations: reproducibility of activation?," vol. 28, no. 8, pp. 733-741, 2007.

[32] H. Sato *et al.*, "Within-subject reproducibility of near-infrared spectroscopy signals in sensorimotor activation after 6 months," vol. 11, no. 1, p. 014021, 2006.

[33] G. Strangman, M. A. Franceschini, and D. A. Boas, "Factors affecting the accuracy of near-infrared spectroscopy concentration calculations for focal changes in oxygenation parameters," vol. 18, no. 4, pp. 865-879, 2003.

[34] G. Strangman, R. Goldstein, S. L. Rauch, and J. Stein, "Near-infrared spectroscopy and imaging for investigating stroke rehabilitation: test-retest reliability and review of the literature," vol. 87, no. 12, pp. 12-19, 2006.

[35] T. J. Huppert, R. D. Hoge, S. G. Diamond, M. A. Franceschini, and D. A. Boas, "A temporal comparison of BOLD, ASL, and NIRS hemodynamic responses to motor stimuli in adult humans," vol. 29, no. 2, pp. 368-382, 2006.

[36] M. L. Schroeter, T. Kupka, T. Mildner, K. Uludağ, and D. Y. von Cramon, "Investigating the post-stimulus undershoot of the BOLD signal—a simultaneous fMRI and fNIRS study," vol. 30, no. 2, pp. 349-358, 2006.

[37] Z. Y. Shan *et al.*, "Modeling of the hemodynamic responses in block design fMRI studies," vol. 34, no. 2, pp. 316-324, 2014.

[38] D. A. Winter, *Biomechanics and motor control of human movement*. John Wiley & Sons, 2009.

[39] K. Khaksari, E. G. Smith, H. O. Miguel, S. Zeytinoglu, N. Fox, and A. H. Gandjbakhche, "An fNIRS Study of Brain Lateralization During Observation and Execution of a Fine Motor Task," vol. 15, 2021.

[40] T. J. Huppert, S. G. Diamond, M. A. Franceschini, and D. A. Boas, "HomER: a review of time-series analysis methods for near-infrared spectroscopy of the brain," vol. 48, no. 10, pp. D280-D298, 2009.

[41] R. Cooper *et al.*, "A systematic comparison of motion artifact correction techniques for functional near-infrared spectroscopy," vol. 6, p. 147, 2012.

[42] H. Dashtestani *et al.*, "Canonical correlation analysis of brain prefrontal activity measured by functional near infra-red spectroscopy (fNIRS) during a moral judgment task," vol. 359, pp. 73-80, 2019.

[43] M. N. Afzal Khan and K. S. Hong, "Most favorable stimulation duration in the sensorimotor cortex for fNIRS-based BCI," *Biomed Opt Express*, vol. 12, no. 10, pp. 5939-5954, Oct 1 2021.

[44] C. Ming, S. Haro, A. M. Simmons, and J. A. Simmons, "A comprehensive computational model of animal biosonar signal processing," vol. 17, no. 2, p. e1008677, 2021.

[45] U. Asgher *et al.*, "Motor Training Using Mental Workload (MWL) With an Assistive Soft Exoskeleton System: A Functional Near-Infrared Spectroscopy (fNIRS) Study for Brain-Machine Interface (BMI)," *Front Neurorobot*, vol. 15, p. 605751, 2021.

[46] M. A. Franceschini, D. K. Joseph, T. J. Huppert, S. G. Diamond, and D. A. Boas, "Diffuse optical imaging of the whole head," vol. 11, no. 5, p. 054007, 2006.

[47] J. W. Barker, A. L. Rosso, P. J. Sparto, and T. J. Huppert, "Correction of motion artifacts and serial correlations for real-time functional near-infrared spectroscopy," vol. 3, no. 3, p. 031410, 2016.

[48] M. Rybar, R. Poli, and I. Daly, "Decoding of semantic categories of imagined concepts of animals and tools in fNIRS," *J Neural Eng*, vol. 18, no. 4, Apr 27 2021.

[49] A. von Lühmann, A. Ortega-Martinez, D. A. Boas, and M. Yücel, "Using the general linear model to improve performance in fNIRS single trial analysis and classification: a perspective," p. 30, 2020.

[50] M. A. Yücel *et al.*, "Mayer waves reduce the accuracy of estimated hemodynamic response functions in functional near-infrared spectroscopy," vol. 7, no. 8, pp. 3078-3088, 2016.

[51] L. Duan, Z. Zhao, Y. Lin, X. Wu, Y. Luo, and P. Xu, "Wavelet-based method for removing global physiological noise in functional near-infrared spectroscopy," *Biomedical optics express*, vol. 9, no. 8, pp. 3805-3820, 2018.

[52] X. Zhang *et al.*, "Activation detection in functional near-infrared spectroscopy by wavelet coherence," vol. 20, no. 1, p. 016004, 2015.

[53] Q. Zhang, G. E. Strangman, and G. Ganis, "Adaptive filtering to reduce global interference in non-invasive NIRS measures of brain activation: how well and when does it work?," *Neuroimage*, vol. 45, no. 3, pp. 788-794, 2009.

[54] R. B. Saager and A. J. Berger, "Direct characterization and removal of interfering absorption trends in two-layer turbid media," vol. 22, no. 9, pp. 1874-1882, 2005.

[55] L. Gagnon, K. Perdue, D. N. Greve, D. Goldenholz, G. Kaskhedikar, and D. A. Boas, "Improved recovery of the hemodynamic response in diffuse optical imaging using short optode separations and state-space modeling," *Neuroimage*, vol. 56, no. 3, pp. 1362-1371, 2011.

[56] L. Gagnon, M. A. Yücel, D. A. Boas, and R. J. Cooper, "Further improvement in reducing superficial contamination in NIRS using double short separation measurements," *Neuroimage*, vol. 85, pp. 127-135, 2014.

[57] R. B. Saager and A. J. Berger, "Measurement of layer-like hemodynamic trends in scalp and cortex: implications for physiological baseline suppression in functional near-infrared spectroscopy," *Journal of biomedical optics*, vol. 13, no. 3, p. 034017, 2008.

[58] R. B. Saager, N. L. Telleri, and A. J. Berger, "Two-detector corrected near infrared spectroscopy (C-NIRS) detects hemodynamic activation responses more robustly than single-detector NIRS," *Neuroimage,* vol. 55, no. 4, pp. 1679-1685, 2011.

[59] T. Takahashi, Y. Takikawa, R. Kawagoe, S. Shibuya, T. Iwano, and S. Kitazawa, "Influence of skin blood flow on near-infrared spectroscopy signals measured on the forehead during a verbal fluency task," *Neuroimage,* vol. 57, no. 3, pp. 991-1002, Aug 1 2011.

[60] Y. Zhang *et al.*, "Multiregional functional near-infrared spectroscopy reveals globally symmetrical and frequency-specific patterns of superficial interference," *Biomed Opt Express,* vol. 6, no. 8, pp. 2786-802, Aug 1 2015.

[61] L. Duan, Z. Zhao, Y. Lin, X. Wu, Y. Luo, and P. Xu, "Wavelet-based method for removing global physiological noise in functional near-infrared spectroscopy," *Biomed Opt Express,* vol. 9, no. 8, pp. 3805-3820, Aug 1 2018.

[62] T. Wilcox, H. Bortfeld, R. Woods, E. Wruck, and D. A. Boas, "Hemodynamic response to featural changes in the occipital and inferior temporal cortex in infants: a preliminary methodological exploration," *Dev Sci,* vol. 11, no. 3, pp. 361-70, May 2008.

[63] T. Wilcox, J. A. Haslup, and D. A. Boas, "Dissociation of processing of featural and spatiotemporal information in the infant cortex," *Neuroimage,* vol. 53, no. 4, pp. 1256-63, Dec 2010.

[64] Y. Zhang, D. H. Brooks, M. A. Franceschini, and D. A. Boas, "Eigenvector-based spatial filtering for reduction of physiological interference in diffuse optical imaging," vol. 10, no. 1, p. 011014, 2005.

[65] S. Kohno *et al.*, "Removal of the skin blood flow artifact in functional near-infrared spectroscopic imaging data through independent component analysis," *J Biomed Opt,* vol. 12, no. 6, p. 062111, Nov-Dec 2007.

[66] H. Zhang, Y. J. Zhang, C. M. Lu, S. Y. Ma, Y. F. Zang, and C. Z. Zhu, "Functional connectivity as revealed by independent component analysis of resting-state fNIRS measurements," (in eng), *Neuroimage,* vol. 51, no. 3, pp. 1150-61, Jul 1 2010.

[67] J. Virtanen, T. Noponen, and P. Meriläinen, "Comparison of principal and independent component analysis in removing extracerebral interference from

near-infrared spectroscopy signals," (in eng), *J Biomed Opt,* vol. 14, no. 5, p. 054032, Sep-Oct 2009.

[68] C. B. Akgül, A. Akin, and B. Sankur, "Extraction of cognitive activity-related waveforms from functional near-infrared spectroscopy signals," vol. 44, no. 11, pp. 945-958, 2006.

[69] I. Schelkanova and V. Toronov, "Independent component analysis of broadband near-infrared spectroscopy data acquired on adult human head," vol. 3, no. 1, pp. 64-74, 2012.

[70] H. Santosa, M. Jiyoun Hong, S.-P. Kim, and K.-S. Hong, "Noise reduction in functional near-infrared spectroscopy signals by independent component analysis," vol. 84, no. 7, p. 073106, 2013.

[71] H.-D. Nguyen, S.-H. Yoo, M. R. Bhutta, and K.-S. Hong, "Adaptive filtering of physiological noises in fNIRS data," vol. 17, no. 1, pp. 1-23, 2018.

[72] C. Büchel and K. Friston, "Dynamic changes in effective connectivity characterized by variable parameter regression and Kalman filtering," vol. 6, no. 5-6, pp. 403-408, 1998.

[73] C. McGilchrist and R. Sandland, "Recursive estimation of the general linear model with dependent errors," vol. 41, no. 1, pp. 65-68, 1979.

[74] E. Bagarinao, K. Matsuo, T. Nakai, and S. Sato, "Estimation of general linear model coefficients for real-time application," vol. 19, no. 2, pp. 422-429, 2003.

[75] B. Molavi and G. A. Dumont, "Wavelet-based motion artifact removal for functional near-infrared spectroscopy," (in eng), *Physiol Meas,* vol. 33, no. 2, pp. 259-70, Feb 2012.

[76] T. Nakano, H. Watanabe, F. Homae, and G. Taga, "Prefrontal cortical involvement in young infants' analysis of novelty," (in eng), *Cereb Cortex,* vol. 19, no. 2, pp. 455-63, Feb 2009.

[77] M. Izzetoglu, A. Devaraj, S. Bunce, and B. Onaral, "Motion artifact cancellation in NIR spectroscopy using Wiener filtering," (in eng), *IEEE Trans Biomed Eng,* vol. 52, no. 5, pp. 934-8, May 2005.

[78] Y. Zhang, J. Sun, and P. Rolfe, "Reduction of global interference in functional multidistance near-infrared spectroscopy using empirical mode decomposition and recursive least squares: a Monte Carlo study," *Journal of the European Optical Society-Rapid publications,* vol. 6, 2011.

[79] Y. Tong, K. P. Lindsey, and B. deB Frederick, "Partitioning of physiological noise signals in the brain with concurrent near-infrared spectroscopy and fMRI," vol. 31, no. 12, pp. 2352-2362, 2011.

[80] H. Tsunashima, K. Yanagisawa, and M. Iwadate, *Measurement of brain function using near-infrared spectroscopy (NIRS)*. InTech, 2012.

[81] R. E. Kalman, "A new approach to linear filtering and prediction problems," 1960.

[82] Y. S. Kim and K. S. Hong, "An IMM algorithm with federated information mode-matched filters for AGV," vol. 21, no. 7, pp. 533-555, 2007.